arXiv:2108.04062v1 [cs.LG] 5 Aug 2021

Householder Activations for Provable Robustness against Adversarial Attacks

Sahil Singla, Surbhi Singla, Soheil Feizi
Department of Computer Science
University of Maryland, College Park
{ssingla,sfeizi}@umd.edu, surbhisingla1995@gmail.com

Abstract

Training convolutional neural networks (CNNs) with a strict Lipschitz constraint under the l_2 norm is useful for provable adversarial robustness, interpretable gradients and stable training. While 1-Lipschitz CNNs can be designed by enforcing a 1-Lipschitz constraint on each layer, training such networks requires each layer to have an orthogonal Jacobian matrix (for all inputs) to prevent gradients from vanishing during backpropagation. A layer with this property is said to be Gradient Norm Preserving (GNP). To construct expressive GNP activation functions, we first prove that the Jacobian of any GNP piecewise linear function is only allowed to change via Householder (HH) transformations for the function to be continuous. Building on this result, we introduce a class of nonlinear GNP activations with learnable Householder transformations called Householder activations. A householder activation parameterized by the vector $\mathbf{v}$ outputs $(\mathbf{I} - 2\mathbf{v}\mathbf{v}^T)\mathbf{z}$ for its input $\mathbf{z}$ if $\mathbf{v}^T\mathbf{z} \leq 0$; otherwise it outputs $\mathbf{z}$. Existing GNP activations such as MaxMin can be viewed as special cases of HH activations for certain settings of these transformations. Thus, networks with HH activations have higher expressive power than those with MaxMin activations. Although networks with HH activations have nontrivial provable robustness against adversarial attacks, we further boost their robustness by (i) introducing a certificate regularization and (ii) relaxing orthogonalization of the last layer of the network. Our experiments on CIFAR-10 and CIFAR-100 show that our regularized networks with HH activations lead to significant improvements in both the standard and provable robust accuracy over the prior works (gain of 3.65% and 4.46% on CIFAR-100 respectively).

1 Introduction

Given a neural network $f : \mathbb{R}^d \to \mathbb{R}^k$, the Lipschitz constant[1] $\mathrm{Lip}(f)$ enforces an upper bound on how much the output is allowed to change in proportion to a change in the input. Previous work has demonstrated that a small Lipschitz constant is useful for improved adversarial robustness [Szegedy et al., 2014, Cissé et al., 2017], generalization bounds [Bartlett et al., 2017, Long and Sedghi, 2020], interpretable gradients [Tsipras et al., 2018] and Wasserstein distance estimation [Villani, 2008]. $\mathrm{Lip}(f)$ also upper bounds the increase in the norm of gradient during backpropagation and can thus prevent gradient explosion during training, enabling us to train very deep networks [Xiao et al., 2018]. While heuristic methods to enforce Lipschitz constraints [Miyato et al., 2018, Gulrajani et al., 2017] have achieved much practical success, they do not provably enforce a bound on $\mathrm{Lip}(f)$ globally and it remains challenging to achieve similar results when $\mathrm{Lip}(f)$ is provably bounded.

Using the property: $\mathrm{Lip}(g \circ h) \leq \mathrm{Lip}(g)\ \mathrm{Lip}(h)$, the Lipschitz constant of the neural network can be bounded by the product of the Lipschitz constant of all layers. While this allows us to construct

[1]Unless specified, we assume the Lipschitz constant under the l_2 norm in this work.

Preprint. Under review.

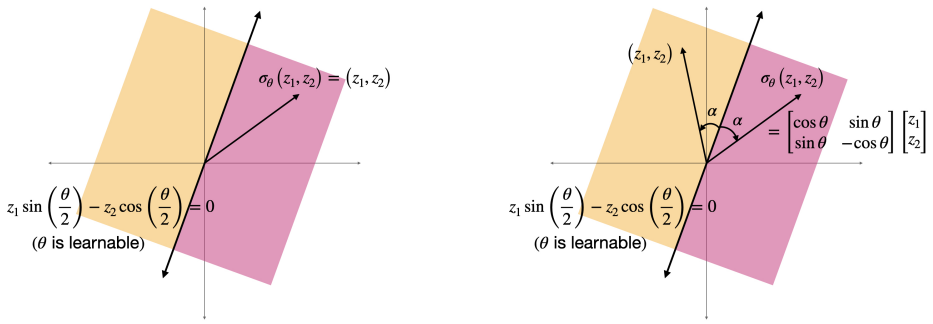

(a) Case 1: $z_1 \sin(\theta/2) - z_2 \cos(\theta/2) > 0$ (b) Case 2: $z_1 \sin(\theta/2) - z_2 \cos(\theta/2) \leq 0$

Figure 1: Illustration of the Householder activation, σ_θ. In each colored region, σ_θ is linear. The Jacobian is $\mathbf{I}$ when (z_1, z_2) lies in the pink region (Case 1) and $\mathbf{I} - 2\mathbf{v}\mathbf{v}^T$ in the other region (Case 2) where $\mathbf{v} = [\sin(\theta/2) \quad -\cos(\theta/2)]^T$. Both of these matrices are orthogonal implying σ_θ is GNP.

1-Lipschitz neural networks by constraining each layer to be 1-Lipschitz, Anil et al. [2018] identified a key difficulty with this approach. Because a 1-Lipschitz layer can only reduce the norm of gradient during backpropagation, backprop through each layer reduces the gradient norm, resulting in small gradient values for layers closer to the input, making training slow and difficult. To address this problem, they introduce Gradient Norm Preserving (GNP) architectures where each layer preserves the gradient norm during backpropagation. This involves constraining the Jacobian of each linear layer to be an orthogonal matrix and using a GNP activation function called $\mathrm{GroupSort}$.

$\mathrm{GroupSort}$ activation function[Anil et al., 2018] first separates the vector of preactivations $\mathbf{z} \in \mathbb{R}^m$ into groups of pre-specified sizes, sorts each group in the descending order and then concatenates these sorted groups. Since these operations can only permute the elements of $\mathbf{z}$, the Jacobian $\nabla_{\mathbf{z}} \mathrm{GroupSort}$ is always a permutation matrix (thus orthogonal), making $\mathrm{GroupSort}$ 1-Lipschitz and GNP. When the group size is 2, the resulting activation function is called MaxMin. MaxMin activation has been widely used in designing provably 1-Lipschitz Convolutional Neural Networks (CNNs) achieving impressive results for deterministic provable adversarial robustness on CIFAR-10.

For 1-Lipschitz CNNs, the robustness certificate for a sample $\mathbf{x}$ from class l is computed as $\mathcal{M}_f(\mathbf{x})/\sqrt{2}$ where $\mathcal{M}_f(\mathbf{x}) = f_l(\mathbf{x}) - \max_{i \neq l} f_i(\mathbf{x})$. Naturally, larger values of $f_l(\mathbf{x})$ and smaller values of $\max_{j \neq l} f_j(\mathbf{x})$ will lead to larger certificates. However, a limitation of MaxMin is that given an input $(z_1, z_2) \in \mathbb{R}^2$, the output is either (z_1, z_2) or (z_2, z_1) and the absolute values of output elements lie between $\min(|z_1|, |z_2|)$ and $\max(|z_2|, |z_1|)$. This bounds the activation values and hence the class logits, thereby limiting the final robustness certificates. One could scale the outputs but then the resulting function is no longer 1-Lipschitz and the certificate $\mathcal{M}_f(\mathbf{x})/\sqrt{2}$ is not valid.

To address this limitation, we introduce a new class of activation functions based on the *Householder* (HH) transformations. Recall that given $\mathbf{z} \in \mathbb{R}^m$, the HH transformation is a linear function reflecting $\mathbf{z}$ about the hyperplane $\mathbf{v}^T\mathbf{x} = 0$ ($\|\mathbf{v}\|_2 = 1$), given by $(\mathbf{I} - 2\mathbf{v}\mathbf{v}^T)\mathbf{z}$ where $\mathbf{I} - 2\mathbf{v}\mathbf{v}^T$ is orthogonal because $\|\mathbf{v}\|_2 = 1$. In this paper, we introduce a nonlinear *Householder* activation defined below:

$$\sigma_{\mathbf{v}}(\mathbf{z}) = \begin{cases} \mathbf{z}, & \mathbf{v}^T\mathbf{z} > 0, \\ (\mathbf{I} - 2\mathbf{v}\mathbf{v}^T)\mathbf{z}, & \mathbf{v}^T\mathbf{z} \leq 0. \end{cases} \tag{1}$$

First, note that since $\mathbf{z} = (\mathbf{I} - 2\mathbf{v}\mathbf{v}^T)\mathbf{z}$ along $\mathbf{v}^T\mathbf{z} = 0$, $\sigma_{\mathbf{v}}$ is continuous. Moreover, the Jacobian $\nabla_{\mathbf{z}}\, \sigma_{\mathbf{v}}$ is either $\mathbf{I}$ or $\mathbf{I} - 2\mathbf{v}\mathbf{v}^T$ (both orthogonal) implying $\sigma_{\mathbf{v}}$ is GNP. Since these properties hold $\forall\, \mathbf{v} : \|\mathbf{v}\|_2 = 1$, $\mathbf{v}$ can be learned during the training, enhancing the expressive power of the network. In fact, we prove that any GNP piecewise linear function that changes from $\mathbf{Q}_1\mathbf{z}$ to $\mathbf{Q}_2\mathbf{z}$ ($\mathbf{Q}_1, \mathbf{Q}_2$ are square orthogonal matrices) along $\mathbf{v}^T\mathbf{z} = 0$ must satisfy $\mathbf{Q}_2 = \mathbf{Q}_1\left(\mathbf{I} - 2\mathbf{v}\mathbf{v}^T\right)$ to be continuous (Theorem 1). That is, HH transformations are *necessary* for any such function to be continuous.

However, a limitation of using $\sigma_{\mathbf{v}}$ directly is that it has only 2 linear regions and is thus limited in its expressive power[2]. To increase the expressive power, we separate the preactivation vector $\mathbf{z} \in \mathbb{R}^m$

[2]We use the number of linear regions as a heuristic for the model's expressive power [Montufar et al., 2014].

into $m/2$ groups of size 2 each and apply $\sigma_{\mathbf{v}}$ on each group where $\mathbf{v}$ ($\in \mathbb{R}^2$) is allowed to be different for each group. Since each group has 2 linear regions, we get $2^{m/2}$ linear regions (same number as MaxMin). When $\mathbf{v} \in \mathbb{R}^2$, without loss of generality, we can set $\mathbf{v} = [\sin(\theta/2) \quad -\cos(\theta/2)]^T$ so that θ becomes the learnable parameter. The resulting function denoted by σ_θ (demonstrated in Figure 1) can be obtained by substituting $\mathbf{v}$ and $\mathbf{I} - 2\mathbf{v}\mathbf{v}^T$ in equation (1) as below:

$$\mathbf{v} = [\sin(\theta/2) \quad -\cos(\theta/2)]^T \quad \implies \quad \mathbf{I} - 2\mathbf{v}\mathbf{v}^T = \begin{bmatrix} \cos\theta & \sin\theta \\ \sin\theta & -\cos\theta \end{bmatrix} \tag{2}$$

For any input (z_1, z_2), the absolute values of the output elements of $\sigma_\theta(z_1, z_2)$ lie between 0 and $r = \sqrt{z_1^2 + z_2^2}$ (in contrast to $\min(|z_1|, |z_2|),\ \max(|z_1|, |z_2|)$ for MaxMin)[3]. Since the activation is applied at each layer, when the number of layers is large, this can significantly increase the range of activation values and thus the final robustness certificates. Moreover, σ_θ is equivalent to MaxMin for $\theta = \pi/2$ implying that it is at least as expressive as MaxMin.

Another limitation of existing 1-Lipschitz CNNs [Li et al., 2019b, Trockman and Kolter, 2021, Singla and Feizi, 2021] is that their robustness guarantees do not scale properly with the l_2 radius ρ. For example, the provable robust accuracy of [Singla and Feizi, 2021] drops $\sim 30\%$ at $\rho = 108/255$ compared to $36/255$ on CIFAR-10 (Table 1). Moreover, these methods also perform poorly when the number of classes is large compared to 10 in the usually studied datasets: MNIST, Fashion MNIST, CIFAR-10 [LeCun and Cortes, 2010, Xiao et al., 2017, Krizhevsky, 2009]. For example, on CIFAR-100 (with 100 classes), the best reported standard accuracy using 1-Lipschitz CNNs is 43.71% (vs 76.68% for CIFAR-10) [Singla and Feizi, 2021].

To address these limitations, we first introduce a regularizer (Section 5.1) that when used with our σ_θ activation on CIFAR-10 dataset, (i) minimally reduces the standard accuracy (max drop of -0.56%) and (ii) significantly enhances the provable robust accuracy for large $\rho = 108/255$ (min gain of $+4.96\%$) across different architectures (Table 1). Next, we introduce a procedure to certify robustness without orthogonalizing the last layer of the network, thereby increasing its expressive power (Section 5.2). On CIFAR-100, this significantly improves both the standard ($> 3\%$) and provable robust accuracy ($> 4\%$ at $\rho = 36/255$) across multiple 1-Lipschitz CNN architectures (Table 2).

In summary, in this paper, we make the following contributions:

- We prove that Householder transformations are *necessary* for any GNP piecewise linear function to be continuous. That is, if such a function changes from $\mathbf{Q}_1\mathbf{z}$ to $\mathbf{Q}_2\mathbf{z}$ along $\mathbf{v}^T\mathbf{z} = 0$, (where $\|\mathbf{v}\|_2 = 1$), then $\mathbf{Q}_2 = \mathbf{Q}_1\left(\mathbf{I} - 2\mathbf{v}\mathbf{v}^T\right)$ (Theorem 1).
- We introduce a class of piecewise linear GNP activation functions with learnable Householder transformations called Householder or HH activations. For certain settings of these transformations, HH activations are equivalent to the existing GNP activations in the literature and thus have higher expressive power, resulting in their superior performance (Tables 1 and 2).
- We introduce a regularizer that when used with our Householder activation significantly advances the provable robust accuracy with a small reduction in standard accuracy. Using LipConvnet-15 network on CIFAR-10, we achieve $+5.81\%$ improvement in provable robust accuracy (at $\rho = 108/255$) with only a -0.29% drop in standard accuracy over the existing methods (Table 1).
- We introduce a certification procedure without orthogonalizing the last linear layer that significantly enhances the standard and provable robust accuracy when the number of classes is large. Using the LipConvnet-15 network on CIFAR-100, our modification achieves gain of $+4.71\%$ in provable robust accuracy (at $\rho = 36/255$) with a gain of $+4.80\%$ in standard accuracy (Table 2).

2 Related work

Provably Lipschitz convolutional neural networks: The class of fully connected neural networks (FCNs) which are Gradient Norm Preserving (GNP) and 1-Lipschitz were first introduced by Anil et al. [2018]. They orthogonalize weight matrices and use $\mathrm{GroupSort}$ as the activation function to design each layer to be GNP. While there have been numerous works on enforcing Lipschitz

[3]To see this, consider $(z_1, z_2) = r\,(\cos\theta, \sin\theta)$ or $-r\,(\cos\theta, \sin\theta)$. Using equations (1) and (2), the Jacobian will be $\mathbf{I} - 2\mathbf{v}\mathbf{v}^T$ for one of them with the output $(r, 0)$ or $(-r, 0)$ respectively.

constraints on convolution layers [Cissé et al., 2017, Tsuzuku et al., 2018, Qian and Wegman, 2019, Gouk et al., 2020, Sedghi et al., 2019], they either enforce loose Lipschitz bounds or are not scalable to large networks. To ensure that the Lipschitz constraint on convolutional layers is tight, multiple recent works try to construct convolution layers with an orthogonal Jacobian matrix [Li et al., 2019b, Trockman and Kolter, 2021, Singla and Feizi, 2021]. These approaches avoid the aforementioned issues and allow the training of large, provably 1-Lipschitz CNNs while achieving impressive results. While 1-Lipschitz CNNs have achieved much practical success, they still use the original MaxMin activation and there is little work so far in designing novel activation functions that are GNP.

Limitations of 1-Lipschitz convolutional neural networks: While 1-Lipschitz CNNs achieve non-trivial robustness guarantees for the l_2 threat model, they can still be susceptible to other threat models that are imperceptible to humans (such as l_p for $p \geq 3$). Moreover, their standard accuracy is significantly lower ($\sim 20\%$ lower on CIFAR-10) than that achieved by standard Resnet [He et al., 2015] architectures (with no tight Lipschitz guarantees). Moreover, the current models do not perform well on datasets with large image sizes and number of classes such as Imagenet.

Provable defenses against adversarial examples: A provably robust classifier is one for which we can guarantee that the classifier's prediction remains constant within some region around the input. Most of the existing methods for provable robustness either bound the Lipschitz constant of the neural network or the individual layers [Weng et al., 2018, Zhang et al., 2019, 2018, Wong et al., 2018, Wong and Kolter, 2018, Raghunathan et al., 2018, Croce et al., 2019, Singh et al., 2018, Singla and Feizi, 2020, Zhang et al., 2021]. However, these methods do not scale to large and practical networks on the ImageNet dataset [Deng et al., 2009]. To scale to such large networks, randomized smoothing [Liu et al., 2018, Cao and Gong, 2017, Lécuyer et al., 2018, Li et al., 2019a, Cohen et al., 2019, Salman et al., 2019, Levine et al., 2019, Kumar et al., 2020a,b] has been proposed as a *probabilistically certified defense*. However, certifying robustness with high probability requires generating a large number of noisy samples leading to high inference-time computation. In contrast, the defense we propose is deterministic and hence not comparable to randomized smoothing. While Levine and Feizi [2021] provide deterministic robustness certificates using randomized smoothing, their certificates are in the l_1 norm and not directly applicable for the l_2 threat model studied in this work.

3 Notation

For a vector $\mathbf{v}$, $\mathbf{v}_j$ denotes its j^{th} element. For a matrix $\mathbf{A}$, $\mathbf{A}_{j,:}$ and $\mathbf{A}_{:,k}$ denote the j^{th} row and k^{th} column respectively. Both $\mathbf{A}_{j,:}$ and $\mathbf{A}_{:,k}$ are assumed to be column vectors (thus $\mathbf{A}_{j,:}$ is the transpose of j^{th} row of $\mathbf{A}$). $\mathbf{A}_{j,k}$ denotes the element in j^{th} row and k^{th} column of $\mathbf{A}$. $\mathbf{A}_{:j,:k}$ denotes the matrix containing the first j rows and k columns of $\mathbf{A}$. The same rules are directly extended to higher order tensors. $\mathbf{I}$ denotes the identity matrix, $\mathbb{R}$ to denote the field of real numbers. For $\theta \in \mathbb{R}$, $\mathbf{J}^{+}(\theta)$ and $\mathbf{J}^{-}(\theta)$ denote the orthogonal matrices with determinants $+1$ and -1 defined as follows:

$$\mathbf{J}^{+}(\theta) = \begin{bmatrix} \cos\theta & \sin\theta \\ -\sin\theta & \cos\theta \end{bmatrix} \qquad \mathbf{J}^{-}(\theta) = \begin{bmatrix} \cos\theta & \sin\theta \\ \sin\theta & -\cos\theta \end{bmatrix} \tag{3}$$

4 Householder Activation Functions

We know that given $\mathbf{z} \in \mathbb{R}^m$, the Householder (HH) transformation reflects $\mathbf{z}$ about the hyperplane $\mathbf{v}^T\mathbf{x} = 0$ where $\|\mathbf{v}\|_2 = 1$. The linear transformation is given by the equation $(\mathbf{I} - 2\mathbf{v}\mathbf{v}^T)\mathbf{z}$ where $\mathbf{I} - 2\mathbf{v}\mathbf{v}^T$ is orthogonal because $\|\mathbf{v}\|_2 = 1$. Now, consider the nonlinear function $\sigma_{\mathbf{v}}$ defined below:

Definition 1. ***(Householder Activation of Order*** 1***)*** *The activation function $\sigma_{\mathbf{v}} : \mathbb{R}^m \to \mathbb{R}^m$, applied on $\mathbf{z} \in \mathbb{R}^m$, is called the m-dimensional Householder Activation of Order 1:*

$$\sigma_{\mathbf{v}}(\mathbf{z}) = \begin{cases} \mathbf{z}, & \mathbf{v}^T\mathbf{z} > 0, \\ (\mathbf{I} - 2\mathbf{v}\mathbf{v}^T)\mathbf{z}, & \mathbf{v}^T\mathbf{z} \leq 0. \end{cases} \tag{4}$$

Since $\sigma_{\mathbf{v}}$ is linear when $\mathbf{v}^T\mathbf{z} > 0$ or $\mathbf{v}^T\mathbf{z} < 0$, it is also continuous in both cases. At the hyperplane separating the two cases i.e. $\mathbf{v}^T\mathbf{z} = 0$ we have: $(\mathbf{I} - 2\mathbf{v}\mathbf{v}^T)\mathbf{z} = \mathbf{z} - 2(\mathbf{v}^T\mathbf{z})\mathbf{v} = \mathbf{z}$ (both linear functions are equal). Thus, $\sigma_{\mathbf{v}}$ is continuous $\forall\ \mathbf{z} \in \mathbb{R}^m$. Moreover, the Jacobian is either $\mathbf{I}$ or $\mathbf{I} - 2\mathbf{v}\mathbf{v}^T$ which are both square orthogonal matrices. Thus, $\sigma_{\mathbf{v}}$ is also GNP and 1-Lipschitz. Since these properties hold for all $\mathbf{v}$ satisfying $\|\mathbf{v}\|_2 = 1$, $\mathbf{v}$ can be made a learnable parameter.

While the above arguments suggest that HH transformations are *sufficient* to ensure such functions are continuous, we also prove that they are *necessary*. That is, we prove that if a GNP piecewise linear function $g : \mathbb{R}^m \to \mathbb{R}^m$ transitions between different linear functions $\mathbf{Q}_1\mathbf{z}$ and $\mathbf{Q}_2\mathbf{z}$ (in an open set $S \subset \mathbb{R}^m$) along a hyperplane $\mathbf{v}^T\mathbf{z} = 0$ (where $\|\mathbf{v}\|_2 = 1$), then g is continuous in S *if and only if* $\mathbf{Q}_2 = \mathbf{Q}_1(\mathbf{I} - 2\mathbf{v}\mathbf{v}^T)$. This theoretical result provides a general principle for designing piecewise linear GNP activation functions. The formal result is stated in the following Theorem:

Theorem 1. *Given an open set $S \subset \mathbb{R}^m$, orthogonal square matrices $\mathbf{Q}_1 \neq \mathbf{Q}_2$, and vector $\mathbf{v} \in \mathbb{R}^m$ ($\|\mathbf{v}\|_2 = 1$) such that $S \cap \{\mathbf{z} : \mathbf{v}^T\mathbf{z} = 0\} \neq \emptyset$, the function g defined as follows:*

$$g(\mathbf{z}) = \begin{cases} \mathbf{Q}_1\mathbf{z}, & \mathbf{z} \in S, \mathbf{v}^T\mathbf{z} > 0, \\ \mathbf{Q}_2\mathbf{z}, & \mathbf{z} \in S, \mathbf{v}^T\mathbf{z} \leq 0 \end{cases} \tag{5}$$

is continuous in S if and only if $\mathbf{Q}_2 = \mathbf{Q}_1(\mathbf{I} - 2\mathbf{v}\mathbf{v}^T)$.

Proof is in Appendix Section A.1. Note that since the matrix $\mathbf{I} - 2\mathbf{v}\mathbf{v}^T$ has determinant -1, the above theorem necessitates that $\det(\mathbf{Q}_1) = -\det(\mathbf{Q}_2)$ i.e the determinant of the Jacobian must change sign whenever the Jacobian of a piecewise linear GNP activation function changes.

A major limitation of using $\sigma_{\mathbf{v}}$ (equation (4)) directly is that it has only 2 linear regions and is thus limited in its expressive power. In contrast, MaxMin first divides the preactivation $\mathbf{z} \in \mathbb{R}^m$ (assuming m is divisible by 2) into $m/2$ groups of size 2 each. Since each group has 2 linear regions, we get $2^{m/2}$ linear regions from the $m/2$ groups. Thus, to increase the expressive power, we similarly divide $\mathbf{z}$ into $m/2$ groups of size 2 each and apply the 2-dimensional Householder activation function of Order 1 to each group resulting in $2^{m/2}$ linear regions (same as MaxMin). Setting $m = 2,\ \mathbf{Q}_1 = \mathbf{I},\ \mathbf{v} = [\sin(\theta/2),\ -\cos(\theta/2)]^T$ in Theorem 1, we get the following activation:

Corollary 1. *The function $\sigma_\theta : \mathbb{R}^2 \to \mathbb{R}^2$ defined as*

$$\sigma_\theta\left(z_1, z_2\right) = \begin{cases} \begin{bmatrix} 1 & 0 \\ 0 & 1 \end{bmatrix} \begin{bmatrix} z_1 \\ z_2 \end{bmatrix} & \text{if } \ z_1 \sin\left(\theta/2\right) - z_2 \cos\left(\theta/2\right) > 0 \\ \begin{bmatrix} \cos\theta & \sin\theta \\ \sin\theta & -\cos\theta \end{bmatrix} \begin{bmatrix} z_1 \\ z_2 \end{bmatrix} & \text{if } \ z_1 \sin\left(\theta/2\right) - z_2 \cos\left(\theta/2\right) \leq 0 \end{cases} \tag{6}$$

is continuous and is called 2D *Householder Activation of Order* 1.

Proof in Appendix A.2. The two cases are demonstrated in Figure 1a and Figure 1b, respectively. Since σ_θ is continuous, GNP and 1-Lipschitz $\forall\ \theta \in \mathbb{R},\ \theta$ is a learnable parameter. For $\theta = \pi/2$ in equation (6), σ_θ is equivalent to MaxMin. Thus, σ_θ is at least as expressive as MaxMin.

To apply σ_θ to the output of a convolution layer $\mathbf{z} \in \mathbb{R}^{m \times n \times n}$ (m is the number of channels and $n \times n$ is the spatial size), we first split $\mathbf{z}$ into 2 tensors along the channel dimension giving the tensors: $\mathbf{z}_{:m/2,:,:}$ and $\mathbf{z}_{m/2:,:,:}$. Each of these tensors is of size $m/2 \times n \times n$ giving $n^2m/2$ groups. We use the same θ for each pair of channels (irrespective of spatial location) resulting in $m/2$ learnable parameters. We initialize each $\theta = \pi/2$ so that σ_θ is equivalent to MaxMin at initialization.

By construction, the output of σ_θ always lies in the pink region (Figure 1) and applying σ_θ again (using the same θ as before) results in the same output: $\sigma_\theta \circ \sigma_\theta = \sigma_\theta$. However, applying σ_ϕ to the output of σ_θ where $\phi \neq \theta + 2m\pi,\ m \in \mathbb{Z}$ further divides the pink region into two regions with different linear functions implying $\sigma_\phi \circ \sigma_\theta \neq \sigma_\theta$ (demonstrated in Figure 2a). Thus, applying σ_θ iteratively n times (using different θ's) allows us to construct HH activations with any number of linear regions. This iterative construction can however be slow when n is large. To address this limitation, we derive an alternative construction of HH activations with any number of linear regions where the linear function needs to be applied only once (not n times!). For this activation function, the linear function (or Jacobian) is determined efficiently based on the region in which the input (z_1, z_2) lies. This construction is given in the following theorem (example in Figure 2b).

Theorem 2. *Given: $0 \leq \theta_0 < \theta_1 \cdots < \theta_{2n} = 2\pi + \theta_0$ such that $\sum_{i=0}^{n-1}(\theta_{2i+1} - \theta_{2i}) = \pi$ and $\alpha_i = 2\sum_{j=0}^{i}\theta_{i-j}(-1)^j$, The function $\sigma_\Theta : \mathbb{R}^2 \to \mathbb{R}^2$ is continuous, GNP and 1-Lipschitz where $\Theta = [\theta_0, \theta_1, \ldots, \theta_{2n-1}]$ (also called* 2D *Householder Activation of order n):*

$$\sigma_\Theta(z_1, z_2) = \begin{bmatrix} \cos\alpha_i & \sin\alpha_i \\ (-1)^i\sin\alpha_i & (-1)^{i+1}\cos\alpha_i \end{bmatrix} \begin{bmatrix} z_1 \\ z_2 \end{bmatrix} \qquad \theta_i \leq \varphi < \theta_{i+1} \tag{7}$$

where $\varphi \in [\theta_0,\ \theta_{2n} = 2\pi + \theta_0)$ and $\cos(\varphi) = z_1/\sqrt{z_1^2 + z_2^2},\ \sin(\varphi) = z_2/\sqrt{z_1^2 + z_2^2}$.

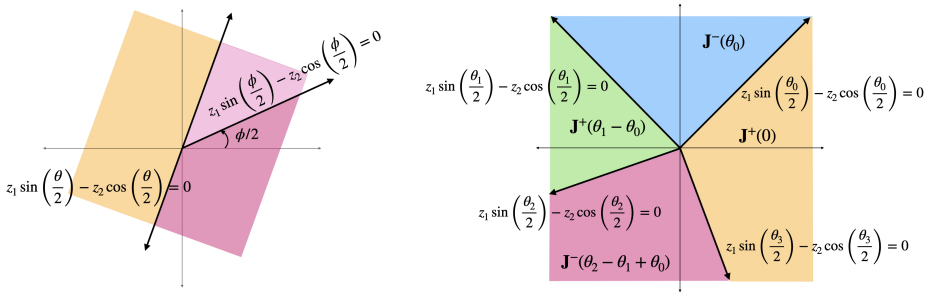

(a) The output of σ_θ always lies in the pink region. Applying σ_ϕ on this where $\phi \neq \theta + 2n\pi, n \in \mathbb{Z}$ further divides this region into two linear regions (light and original pink).

(b) In each colored region, the function is linear with the Jacobian mentioned. For the function to be continuous, we must have $\theta_3 - \theta_2 + \theta_1 - \theta_0 = \pi$. Thus, any 3 of $\{\theta_0, \theta_1, \theta_2, \theta_3\}$ can be chosen as learnable parameters.

Figure 2: Constructing Higher Order Householder activations ($\mathbf{J}^+$ and $\mathbf{J}^-$ defined in equation (3))

Proof is in Appendix Section A.3 and more details about the Theorem in Appendix Section C.

5 Provable Robustness using Householder Activations

We can now construct a 1-Lipschitz neural network, $f : \mathbb{R}^d \to \mathbb{R}^k$ (k is the number of classes) by composing 1-Lipschitz convolution layers and HH activation functions. To certify robustness for some input $\mathbf{x}$ with prediction l, we first define the margin of prediction: $\mathcal{M}_f(\mathbf{x}) = \max(0, f_l(\mathbf{x}) - \max_{i \neq l} f_i(\mathbf{x}))$ where $f_i(\mathbf{x})$ is the logit for class i and l is the correct label. Using Theorem 7 in Li et al. [2019b], we can derive the robustness certificate (in the l_2 norm) as $\mathcal{M}_f(\mathbf{x})/\sqrt{2}$. Thus, the l_2 distance of $\mathbf{x}$ to the decision boundary is lower bounded by $\mathcal{M}_f(\mathbf{x})/\sqrt{2}$:

$$\min_{i \neq l} \min_{f_i(\mathbf{x}^*) = f_l(\mathbf{x}^*)} \|\mathbf{x}^* - \mathbf{x}\|_2 \geq \frac{\mathcal{M}_f(\mathbf{x})}{\sqrt{2}}$$

5.1 Certificate Regularization

Our goal is to maximize the certificate $\mathcal{M}_f(\mathbf{x})/\sqrt{2}$ for correctly classified inputs $\mathbf{x}$. However, a limitation of using cross entropy loss during training is that it is not explicitly designed to maximize the margin $\mathcal{M}_f(\mathbf{x})$ and thus, the robustness certificate. That is, once the cross entropy loss becomes small, the gradients will no longer try to further increase the margin $\mathcal{M}_f(\mathbf{x})$ even though the network may have the capacity to learn bigger margins. To address this limitation, we add a regularization term to increase the robustness certificate per input to the usual cross entropy loss:

$$\min_{\Omega} \quad \mathbb{E}_{(\mathbf{x},l)\sim D}\left[\ell\left(f_\Omega(\mathbf{x}), l\right) - \gamma \operatorname{relu}\left(\frac{\mathcal{M}_f(\mathbf{x})}{\sqrt{2}}\right)\right] \tag{8}$$

In the above equation, f_Ω denotes the 1-Lipschitz neural network parametrized by Ω, $f_\Omega(\mathbf{x})$ denotes the logits for the input $\mathbf{x}$, $\ell\left(f_\Omega(\mathbf{x}), l\right)$ is the cross entropy loss for input $\mathbf{x}$ with label l and $\gamma > 0$ is the regularization coefficient for maximizing the certificate. We have the minus sign in front of the regularization term γ relu$(\mathcal{M}_f(\mathbf{x})/\sqrt{2})$ because we want to *maximize* the certificate while *minimizing* the cross entropy loss. For wrongly classified inputs, $\mathcal{M}_f(\mathbf{x})/\sqrt{2} < 0 \implies \text{relu}(\mathcal{M}_f(\mathbf{x})/\sqrt{2}) = 0$. This ensures that the optimization tries to increase the certificates *only* for the correctly classified inputs. We call the above mentioned procedure *Certificate Regularization* (abbreviated as *CR*).

5.2 Last Layer Normalization

Existing 1-Lipschitz neural networks constrain the weight matrices of all linear layers of the network to be orthogonal to ensure they are GNP. For the last weight matrix, $\mathbf{W} \in \mathbb{R}^{k \times m}$ (k is the number of classes, m is the dimension of the penultimate layer, $m > k$), this enforces the following constraints:

$$\forall j, \ \|\mathbf{W}_{j,:}\|_2 = 1, \qquad i \neq j, \ \ \mathbf{W}_{j,:} \perp \mathbf{W}_{i,:}$$

Now suppose that for some input $\mathbf{x}$ with label l, we want to update $\mathbf{W}$ to increase the logit for the l^{th} class. Since $\|\mathbf{W}_{l,:}\|_2$ is constrained to be 1, the logit can only be increased by changing the direction of the vector $\mathbf{W}_{l,:}$. Because the other rows $\{\mathbf{W}_{i,:},\ i \neq l\}$ are constrained to be orthogonal to $\mathbf{W}_{l,:}$, this further requires an update for all the rows of $\mathbf{W}$. This has the negative effect that during training, any update made to learn some class may necessitate the forgetting of information relevant for the other classes. This can be particularly problematic when the number of classes k is large (such as in CIFAR-100) and thus the number of orthogonality constraints per row i.e. $k-1$ is large.

To address this limitation, we propose to keep the last layer unchanged i.e. not enforce the orthogonality constraints and use the following theorem to compute the robustness certificate:

Theorem 3. *Given* 1*-Lipschitz continuous function* $g : \mathbb{R}^d \to \mathbb{R}^m$ *and* $\mathbf{W} \in \mathbb{R}^{k \times m},\ \mathbf{b} \in \mathbb{R}^k$ *(*k *is the number of classes), construct a new function* $f : \mathbb{R}^d \to \mathbb{R}^k$ *defined as:* $f(\mathbf{x}) = \mathbf{W}g(\mathbf{x}) + \mathbf{b}$*. Let* $f_l(\mathbf{x}) > \max_{i \neq l} f_i(\mathbf{x})$*. The robustness certificate (under the* l_2 *norm) is given by:*

$$\min_{i \neq l} \min_{f_l(\mathbf{x}^*) = f_i(\mathbf{x}^*)} \|\mathbf{x}^* - \mathbf{x}\|_2 \ \geq \min_{i \neq l} \frac{f_l(\mathbf{x}) - f_i(\mathbf{x})}{\|\mathbf{W}_{l,:} - \mathbf{W}_{i,:}\|_2}$$

Proof is in Appendix Section A.4. In our experiments, we observe that using the last layer without orthogonalization often results in large norms of row vectors $\|\mathbf{W}_{i,:}\|_2$, thus large values of $\|\mathbf{W}_{l,:} - \mathbf{W}_{i,:}\|_2$ and smaller certificates (Theorem 3). To address this problem, we normalize all rows to be of unit norm before computing the logits. While each row $\mathbf{W}_{i,:}$ is still constrained to be of unit norm, their directions are allowed to change freely. This provides significant improvements when the number of classes is large. We call this procedure *Last Layer Normalization* (abbreviated as *LLN*).

6 Experiments

We perform experiments under the setting of provably robust image classification on CIFAR-10 and CIFAR-100 datasets using the same 1-Lipschitz CNN architectures used by Singla and Feizi [2021] (LipConvnet-5, 10, 15, ..., 40) due to their superior performance over the prior works. We compare with the three orthogonal convolution layers in the literature: SOC [Singla and Feizi, 2021], BCOP [Li et al., 2019b] and Cayley [Trockman and Kolter, 2021] using MaxMin as the activation function. We use SOC with MaxMin as the primary baseline for comparison in the maintext due to their superior performance over prior works (BCOP, Cayley). Results using BCOP and Cayley convolutions are given in Appendix Sections E and F for completeness. We use the same implementations for these convolution layers as given in their respective github repositories. We compare the provable robust accuracy using 3 different values of the l_2 perturbation radius $\rho = 36/255,\ 72/255,\ 108/255$. In both Tables 1 and 2, for all networks, we use SOC as the convolution layer. The symbol HH (in Tables 1, 2) is for the 2D Householder Activation of order 1 or σ_θ (defined in equation (6)). We observe negligible inference time overhead due to any of our changes (Appendix Tables 3, 9).

All experiments were performed using 1 NVIDIA GeForce RTX 2080 Ti GPU. All networks were trained for 200 epochs with initial learning rate of 0.1, dropped by a factor of 0.1 after 100 and 150 epochs. For Certificate Regularization (or CR), we set the parameter $\gamma = 0.1$.

6.1 Results on CIFAR-10

In Table 1, for each architecture, the row "SOC + MaxMin" uses the MaxMin activation, the row "+ HH" uses σ_θ activation (replacing MaxMin) and the row "+ CR" also adds Certificate Regularization with $\gamma = 0.1$ (again using σ_θ as the activation). Due to the small number of classes in CIFAR-10, we do not observe significant gains using Last Layer Normalization or LLN (Appendix Table 7). Thus, we do not include LLN for any of the results in Table 1. The column, "Increase $(108/255)$" denotes the increase in provable robust accuracy with $\rho = 108/255$ relative to "SOC + MaxMin".

For LipConvnet-$25, 30, 35, 40$ architectures, we observe gains in both the standard and provable robust accuracy by replacing MaxMin with the HH activation (i.e σ_θ). The gains in provable robust accuracy ($\rho = 108/255$) are significantly higher for deeper networks: LipConvnet-35 (3.65%) and LipConvnet-40 (4.35%) with decent gains in standard accuracy (1.71 and 1.61% respectively). We show the results of using 2D Householder activation function of order 2 in Appendix Table 6. We do not observe any significant improvements compared to using the order 1, i.e. σ_θ activation.

Architecture	Methods	Standard Accuracy	Provable Robust Acc. ($\rho =$)			Increase
			36/255	72/255	108/255	(108/255)
LipConvnet-5	SOC + MaxMin	75.78%	59.18%	42.01%	27.09%	_
	+ HH	**76.30%**	60.12%	43.20%	27.39%	+0.30%
	+ CR	75.31%	**60.37%**	**45.62%**	**32.38%**	**+5.29%**
LipConvnet-10	SOC + MaxMin	76.45%	60.86%	44.15%	29.15%	_
	+ HH	**76.86%**	61.52%	44.91%	29.90%	+0.75%
	+ CR	76.23%	**62.57%**	**47.70%**	**34.15%**	**+5.00%**
LipConvnet-15	SOC + MaxMin	76.68%	61.36%	44.28%	29.66%	_
	+ HH	**77.41%**	61.92%	45.60%	31.10%	+1.44%
	+ CR	76.39%	**62.96%**	**48.47%**	**35.47%**	**+5.81%**
LipConvnet-20	SOC + MaxMin	76.90%	61.87%	45.79%	31.08%	_
	+ HH	**76.99%**	61.76%	45.59%	30.99%	-0.09%
	+ CR	76.34%	**62.63%**	**48.69%**	**36.04%**	**+4.96%**
LipConvnet-25	SOC + MaxMin	75.24%	60.17%	43.55%	28.60%	_
	+ HH	**76.37%**	61.50%	44.72%	29.83%	+1.23%
	+ CR	75.21%	**61.98%**	**47.93%**	**34.92%**	**+6.32%**
LipConvnet-30	SOC + MaxMin	74.51%	59.06%	42.46%	28.05%	_
	+ HH	**75.25%**	59.90%	43.85%	29.35%	+1.30%
	+ CR	74.23%	**60.64%**	**46.51%**	**34.08%**	**+6.03%**
LipConvnet-35	SOC + MaxMin	73.73%	58.50%	41.75%	27.20%	_
	+ HH	**75.44%**	61.05%	45.38%	30.85%	+3.65%
	+ CR	74.25%	**61.30%**	**47.60%**	**35.21%**	**+8.01%**
LipConvnet-40	SOC + MaxMin	71.63%	54.39%	37.92%	24.13%	_
	+ HH	**73.24%**	58.12%	42.24%	28.48%	+4.35%
	+ CR	72.59%	**59.04%**	**44.92%**	**32.87%**	**+8.74%**

Table 1: Results for provable robustness against adversarial examples on the CIFAR-10 dataset. Results with BCOP and Cayley convolutions are in Appendix Tables 4 and 5.

Adding CR further boosts the provable robust accuracy while slightly reducing the standard accuracy. Comparing "+ CR" with "SOC + MaxMin", we observe small drops in standard accuracy for LipConvnet-$5, 10, \ldots, 30$ networks (max. drop of -0.56%), and gains for LipConvnet-35 ($+0.52\%$) and LipConvnet-40 ($+0.96\%$). For provable robust accuracy ($\rho = 108/255$), we observe very significant gains of $> 4.96\%$ for all networks and $> 8\%$ for the deeper LipConvnet-35, 40 networks.

6.2 Results on CIFAR-100

In Table 2, for each architecture, the row "SOC + MaxMin" uses the MaxMin activation, "+ LLN" adds Last Layer Normalization (uses MaxMin), "+ HH" replaces MaxMin with σ_θ (also uses LLN) , "+ CR" also adds Certificate Regularization with $\gamma = 0.1$ (uses both σ_θ and LLN). The column, "Increase (Standard)" denotes the increase in standard accuracy relative to "SOC + MaxMin".

By adding LLN (the row "+ LLN"), we observe gains in standard (min gain of 1.10%) and provable robust accuracy (min gain of 1.71% at $\rho = 36/255$) across all the LipConvnet architectures (gains relative to "SOC + MaxMin"). These gains are smallest for the LipConvnet-40 network with the maximum depth. However, replacing MaxMin with the σ_θ activation further improves the standard (min gain of 3.65%) and provable robust accuracy (min gain of 4.46% at $\rho = 36/255$) across all networks (again relative to "SOC + MaxMin"). Similar to what we observed for CIFAR-10, replacing MaxMin with σ_θ significantly improves the performance of the deeper LipConvnet-$35, 40$ networks.

Architecture	Methods	Standard Accuracy	Provable Robust Acc. ($\rho =$) 36/255	72/255	108/255	Increase (Standard)
LipConvnet-15	SOC + MaxMin	42.92%	28.81%	17.93%	10.73%	_
	+ LLN	47.72%	33.52%	21.89%	13.76%	+4.80%
	+ HH	**47.72%**	33.97%	22.45%	13.81%	**+4.80%**
	+ CR	47.61%	**34.54%**	**23.16%**	**15.09%**	+4.69%
LipConvnet-20	SOC + MaxMin	43.06%	29.34%	18.66%	11.20%	_
	+ LLN	46.86%	33.48%	22.14%	14.10%	+3.80%
	+ HH	47.71%	34.22%	22.93%	14.57%	+4.65%
	+ CR	**47.84%**	**34.77%**	**23.70%**	**15.84%**	**+4.78%**
LipConvnet-25	SOC + MaxMin	43.37%	28.59%	18.18%	10.85%	_
	+ LLN	46.32%	32.87%	21.53%	13.86%	+2.95%
	+ HH	**47.70%**	34.00%	22.67%	14.57%	**+4.33%**
	+ CR	46.87%	**34.09%**	**23.41%**	**15.61%**	+3.50%
LipConvnet-30	SOC + MaxMin	42.87%	28.74%	18.47%	11.21%	_
	+ LLN	46.18%	32.82%	21.52%	13.52%	+3.31%
	+ HH	46.80%	33.72%	22.70%	14.31%	+3.93%
	+ CR	**46.92%**	**34.17%**	**23.21%**	**15.84%**	**+4.05%**
LipConvnet-35	SOC + MaxMin	42.42%	28.34%	18.10%	10.96%	_
	+ LLN	45.22%	32.10%	21.28%	13.25%	+2.80%
	+ HH	46.21%	32.80%	21.55%	14.13%	+3.79%
	+ CR	**46.88%**	**33.64%**	**23.34%**	**15.73%**	**+4.46%**
LipConvnet-40	SOC + MaxMin	41.84%	28.00%	17.40%	10.28%	_
	+ LLN	42.94%	29.71%	19.30%	11.99%	+1.10%
	+ HH	**45.84%**	**32.79%**	21.98%	14.07%	**+4.00%**
	+ CR	45.03%	32.57%	**22.37%**	**14.76%**	+3.19%

Table 2: Results for provable robustness against adversarial examples on the CIFAR-100 dataset. Results with LipConvnet-5, 10 are in Appendix Table 8. BCOP, Cayley are in Tables 10, 11.

Similar to CIFAR-10, adding CR further improves the provable robust accuracy while only slightly reducing the standard accuracy. Because LLN significantly improves the standard accuracy, we compare the standard accuracy numbers between rows "+ CR" and "+ LLN" to evaluate the drop due to CR. We observe a small drop in standard accuracy (-0.04%, -0.11%) only for LipConvnet-5 and LipConvnet-15 networks. For the other networks, the standard accuracy actually *increases*.

7 Conclusion

In this work, we prove that the Jacobian of any Gradient Norm Preserving (GNP) piecewise linear function is only allowed to change via Householder transformations for the function to be continuous. This provides a general principle for designing piecewise linear GNP functions. Using this result, we introduce a class of GNP activation functions called Householder (or HH) activations with learnable parameters of Householder transformations. Our HH activations generalize the existing GNP activations in the literature and achieve superior performance in different settings. In addition, we introduce a certificate regularizer and a procedure to certify robustness without orthogonalizing the last linear layer of the network that gives significant gains when combined with our activations. We also derive an efficient construction of HH activations with any arbitrary number of linear regions in 2 dimensions. Our experimental results suggest that constructing expressive HH activation functions in higher dimensions, coming up with better initialization methods and regularizers can further improve the performance of 1-Lipschitz neural networks and are interesting directions of future research.

References

C. Anil, J. Lucas, and R. B. Grosse. Sorting out lipschitz function approximation. In *ICML*, 2018.

P. L. Bartlett, D. J. Foster, and M. Telgarsky. Spectrally-normalized margin bounds for neural networks. In *Proceedings of the 31st International Conference on Neural Information Processing Systems*, NIPS'17, pages 6241–6250, USA, 2017. Curran Associates Inc. ISBN 978-1-5108-6096-4. URL http://dl.acm.org/citation.cfm?id=3295222.3295372.

X. Cao and N. Z. Gong. Mitigating evasion attacks to deep neural networks via region-based classification. In *Proceedings of the 33rd Annual Computer Security Applications Conference*, ACSAC 2017, page 278–287, New York, NY, USA, 2017. Association for Computing Machinery. ISBN 9781450353458. doi: 10.1145/3134600.3134606. URL https://doi.org/10.1145/3134600.3134606.

M. Cissé, P. Bojanowski, E. Grave, Y. N. Dauphin, and N. Usunier. Parseval networks: Improving robustness to adversarial examples. In D. Precup and Y. W. Teh, editors, *Proceedings of the 34th International Conference on Machine Learning, ICML 2017, Sydney, NSW, Australia, 6-11 August 2017*, volume 70 of *Proceedings of Machine Learning Research*, pages 854–863. PMLR, 2017. URL http://proceedings.mlr.press/v70/cisse17a.html.

J. M. Cohen, E. Rosenfeld, and J. Z. Kolter. Certified adversarial robustness via randomized smoothing. In *ICML*, 2019.

F. Croce, M. Andriushchenko, and M. Hein. Provable robustness of relu networks via maximization of linear regions. *AISTATS 2019*, 2019.

J. Deng, W. Dong, R. Socher, L. Li, K. Li, and L. Fei-Fei. Imagenet: A large-scale hierarchical image database. *2009 IEEE Conference on Computer Vision and Pattern Recognition*, pages 248–255, 2009.

H. Gouk, E. Frank, B. Pfahringer, and M. J. Cree. Regularisation of neural networks by enforcing lipschitz continuity, 2020.

I. Gulrajani, F. Ahmed, M. Arjovsky, V. Dumoulin, and A. C. Courville. Improved training of wasserstein gans. In I. Guyon, U. V. Luxburg, S. Bengio, H. Wallach, R. Fergus, S. Vishwanathan, and R. Garnett, editors, *Advances in Neural Information Processing Systems*, volume 30, pages 5767–5777. Curran Associates, Inc., 2017. URL https://proceedings.neurips.cc/paper/2017/file/892c3b1c6dccd52936e27cbd0ff683d6-Paper.pdf.

K. He, X. Zhang, S. Ren, and J. Sun. Deep residual learning for image recognition. *The IEEE Conference on Computer Vision and Pattern Recognition (CVPR)*, pages 770–778, 2015.

A. Krizhevsky. Learning multiple layers of features from tiny images. Technical report, 2009.

A. Kumar, A. Levine, S. Feizi, and T. Goldstein. Certifying confidence via randomized smoothing. In H. Larochelle, M. Ranzato, R. Hadsell, M. F. Balcan, and H. Lin, editors, *Advances in Neural Information Processing Systems*, volume 33, pages 5165–5177. Curran Associates, Inc., 2020a. URL https://proceedings.neurips.cc/paper/2020/file/37aa5dfc44dddd0d19d4311e2c7a0240-Paper.pdf.

A. Kumar, A. Levine, T. Goldstein, and S. Feizi. Curse of dimensionality on randomized smoothing for certifiable robustness. In H. D. III and A. Singh, editors, *Proceedings of the 37th International Conference on Machine Learning*, volume 119 of *Proceedings of Machine Learning Research*, pages 5458–5467. PMLR, 13–18 Jul 2020b. URL http://proceedings.mlr.press/v119/kumar20b.html.

Y. LeCun and C. Cortes. MNIST handwritten digit database. 2010. URL http://yann.lecun.com/exdb/mnist/.

M. Lécuyer, V. Atlidakis, R. Geambasu, D. Hsu, and S. K. K. Jana. Certified robustness to adversarial examples with differential privacy. In *IEEE S&P 2019*, 2018.

A. Levine and S. Feizi. Improved, deterministic smoothing for l1 certified robustness. In *ICML*, 2021.

A. Levine, S. Singla, and S. Feizi. Certifiably robust interpretation in deep learning, 2019.

B. Li, C. Chen, W. Wang, and L. Carin. Certified adversarial robustness with additive noise. In H. Wallach, H. Larochelle, A. Beygelzimer, F. d'Alché-Buc, E. Fox, and R. Garnett, editors, *Advances in Neural Information Processing Systems*, volume 32, pages 9464–9474. Curran Associates, Inc., 2019a. URL https://proceedings.neurips.cc/paper/2019/file/335cd1b90bfa4ee70b39d08a4ae0cf2d-Paper.pdf.

Q. Li, S. Haque, C. Anil, J. Lucas, R. Grosse, and J.-H. Jacobsen. Preventing gradient attenuation in lipschitz constrained convolutional networks. *Conference on Neural Information Processing Systems*, 2019b.

X. Liu, M. Cheng, H. Zhang, and C. Hsieh. Towards robust neural networks via random self-ensemble. In *ECCV*, 2018.

P. M. Long and H. Sedghi. Generalization bounds for deep convolutional neural networks. In *International Conference on Learning Representations*, 2020. URL https://openreview.net/forum?id=r1e_FpNFDr.

T. Miyato, T. Kataoka, M. Koyama, and Y. Yoshida. Spectral normalization for generative adversarial networks. In *International Conference on Learning Representations*, 2018. URL https://openreview.net/forum?id=B1QRgziT-.

G. F. Montufar, R. Pascanu, K. Cho, and Y. Bengio. On the number of linear regions of deep neural networks. In Z. Ghahramani, M. Welling, C. Cortes, N. Lawrence, and K. Q. Weinberger, editors, *Advances in Neural Information Processing Systems*, volume 27. Curran Associates, Inc., 2014. URL https://proceedings.neurips.cc/paper/2014/file/109d2dd3608f669ca17920c511c2a41e-Paper.pdf.

H. Qian and M. N. Wegman. L2-nonexpansive neural networks. In *International Conference on Learning Representations*, 2019. URL https://openreview.net/forum?id=ByxGSsR9FQ.

A. Raghunathan, J. Steinhardt, and P. Liang. Semidefinite relaxations for certifying robustness to adversarial examples. In *NeurIPS*, 2018.

H. Salman, J. Li, I. Razenshteyn, P. Zhang, H. Zhang, S. Bubeck, and G. Yang. Provably robust deep learning via adversarially trained smoothed classifiers. In H. Wallach, H. Larochelle, A. Beygelzimer, F. d'Alché-Buc, E. Fox, and R. Garnett, editors, *Advances in Neural Information Processing Systems*, volume 32, pages 11292–11303. Curran Associates, Inc., 2019. URL https://proceedings.neurips.cc/paper/2019/file/3a24b25a7b092a252166a1641ae953e7-Paper.pdf.

H. Sedghi, V. Gupta, and P. M. Long. The singular values of convolutional layers. In *International Conference on Learning Representations*, 2019. URL https://openreview.net/forum?id=rJevYoA9Fm.

G. Singh, T. Gehr, M. Mirman, M. Püschel, and M. T. Vechev. Fast and effective robustness certification. In *NeurIPS*, 2018.

S. Singla and S. Feizi. Second-order provable defenses against adversarial attacks. In H. D. III and A. Singh, editors, *Proceedings of the 37th International Conference on Machine Learning*, volume 119 of *Proceedings of Machine Learning Research*, pages 8981–8991. PMLR, 13–18 Jul 2020. URL http://proceedings.mlr.press/v119/singla20a.html.

S. Singla and S. Feizi. Skew orthogonal convolutions. In *ICML*, 2021. URL https://arxiv.org/abs/2105.11417.

C. Szegedy, W. Zaremba, I. Sutskever, J. Bruna, D. Erhan, I. Goodfellow, and R. Fergus. Intriguing properties of neural networks. In *International Conference on Learning Representations*, 2014. URL http://arxiv.org/abs/1312.6199.

A. Trockman and J. Z. Kolter. Orthogonalizing convolutional layers with the cayley transform. In *International Conference on Learning Representations*, 2021. URL https://openreview.net/forum?id=Pbj8H_jEHYv.

D. Tsipras, S. Santurkar, L. Engstrom, A. Turner, and A. Madry. Robustness may be at odds with accuracy. In *ICLR*, 2018.

Y. Tsuzuku, I. Sato, and M. Sugiyama. Lipschitz-margin training: Scalable certification of perturbation invariance for deep neural networks. In *NeurIPS*, 2018.

C. Villani. Optimal transport, old and new, 2008.

T.-W. Weng, H. Zhang, H. Chen, Z. Song, C.-J. Hsieh, D. Boning, and I. S. D. A. Daniel. Towards fast computation of certified robustness for relu networks. In *International Conference on Machine Learning (ICML)*, july 2018.

E. Wong and Z. Kolter. Provable defenses against adversarial examples via the convex outer adversarial polytope. In J. Dy and A. Krause, editors, *Proceedings of the 35th International Conference on Machine Learning*, volume 80 of *Proceedings of Machine Learning Research*, pages 5286–5295, Stockholmsmässan, Stockholm Sweden, 10–15 Jul 2018. PMLR. URL http://proceedings.mlr.press/v80/wong18a.html.

E. Wong, F. R. Schmidt, J. H. Metzen, and J. Z. Kolter. Scaling provable adversarial defenses. In *NeurIPS*, 2018.

H. Xiao, K. Rasul, and R. Vollgraf. Fashion-mnist: a novel image dataset for benchmarking machine learning algorithms, 2017.

L. Xiao, Y. Bahri, J. Sohl-Dickstein, S. Schoenholz, and J. Pennington. Dynamical isometry and a mean field theory of CNNs: How to train 10,000-layer vanilla convolutional neural networks. In J. Dy and A. Krause, editors, *Proceedings of the 35th International Conference on Machine Learning*, volume 80 of *Proceedings of Machine Learning Research*, pages 5393–5402, Stockholmsmässan, Stockholm Sweden, 10–15 Jul 2018. PMLR. URL http://proceedings.mlr.press/v80/xiao18a.html.

B. Zhang, T. Cai, Z. Lu, D. He, and L. Wang. Towards certifying linfinity robustness using neural networks with linfinity-dist neurons. In *ICML*, 2021.

H. Zhang, T.-W. Weng, P.-Y. Chen, C.-J. Hsieh, and L. Daniel. Efficient neural network robustness certification with general activation functions. In *Advances in Neural Information Processing Systems (NIPS), arXiv preprint arXiv:1811.00866*, dec 2018.

H. Zhang, P. Zhang, and C.-J. Hsieh. Recurjac: An efficient recursive algorithm for bounding jacobian matrix of neural networks and its applications. In *AAAI Conference on Artificial Intelligence (AAAI), arXiv preprint arXiv:1810.11783*, dec 2019.

A Proofs

A.1 Proof of Theorem 1

Proof. We first prove that if $\mathbf{Q}_2 = (\mathbf{I} - 2\mathbf{v}\mathbf{v}^T)\mathbf{Q}_1$, then the function g is continuous.
First, observe that for $\mathbf{v}^T\mathbf{z} > 0$, $g(\mathbf{z}) = \mathbf{Q}_1\mathbf{z}$ which is continuous.
Similarly, for $\mathbf{v}^T\mathbf{z} < 0$, $g(\mathbf{z}) = \mathbf{Q}_2\mathbf{z}$ which is again continuous.
This proves that the function g is continuous when $\mathbf{v}^T\mathbf{z} > 0$ or $\mathbf{v}^T\mathbf{z} < 0$.
Thus, to prove continuity $\forall\ \mathbf{z} \in S$, we must prove that:

$$\mathbf{Q}_1\mathbf{z} = \mathbf{Q}_2\mathbf{z} \qquad \forall\ \mathbf{z} : \mathbf{v}^T\mathbf{z} = 0 \tag{9}$$

Since $\mathbf{Q}_2 = \mathbf{Q}_1(\mathbf{I} - 2\mathbf{v}\mathbf{v}^T)$, we have:

$$\mathbf{Q}_2 - \mathbf{Q}_1 = -2\mathbf{Q}_1\mathbf{v}\mathbf{v}^T$$
$$(\mathbf{Q}_2 - \mathbf{Q}_1)\,\mathbf{z} = -2\left(\mathbf{Q}_1\mathbf{v}\mathbf{v}^T\right)\mathbf{z} = -2\mathbf{Q}_1\mathbf{v}\left(\mathbf{v}^T\mathbf{z}\right)$$

The above equation directly proves (9).

Now, we prove the other direction i.e if g is continuous in S then, $\mathbf{Q}_2 = \mathbf{Q}_1(\mathbf{I} - 2\mathbf{v}\mathbf{v}^T)$.
Since g is continuous for all $\mathbf{z} : \mathbf{v}^T\mathbf{z} = 0$, we have:

$$\mathbf{Q}_2\mathbf{z} = \mathbf{Q}_1\mathbf{z} \qquad \forall\ \mathbf{z} : \mathbf{v}^T\mathbf{z} = 0$$
$$(\mathbf{Q}_2 - \mathbf{Q}_1)\,\mathbf{z} = \mathbf{0} \qquad \forall\ \mathbf{z} : \mathbf{v}^T\mathbf{z} = 0$$

Since $\mathbf{z} \in \mathbb{R}^m$, we know that the set of vectors: $\{\mathbf{z} : \mathbf{v}^T\mathbf{z} = 0\}$ spans a $m-1$ dimensional subspace.
Thus, the null space of $\mathbf{Q}_2 - \mathbf{Q}_1$ is of size $m-1$.
This in turn implies that $\mathbf{Q}_2 - \mathbf{Q}_1$ is a rank one matrix given by the following equation:

$$\mathbf{Q}_2 - \mathbf{Q}_1 = \mathbf{u}\mathbf{v}^T \tag{10}$$

where the vector $\mathbf{u}$ remains to be determined.
Since $\mathbf{Q}_1$ and $\mathbf{Q}_2$ are orthogonal matrices, we have the following set of equations:

$$\mathbf{Q}_2^T\mathbf{Q}_2 = \left(\mathbf{Q}_1 + \mathbf{u}\mathbf{v}^T\right)^T\left(\mathbf{Q}_1 + \mathbf{u}\mathbf{v}^T\right) \tag{11}$$
$$\mathbf{Q}_2\mathbf{Q}_2^T = \left(\mathbf{Q}_1 + \mathbf{u}\mathbf{v}^T\right)\left(\mathbf{Q}_1 + \mathbf{u}\mathbf{v}^T\right)^T \tag{12}$$

We first simplify equation (11):

$$\mathbf{Q}_2^T\mathbf{Q}_2 = \left(\mathbf{Q}_1^T + \mathbf{v}\mathbf{u}^T\right)\left(\mathbf{Q}_1 + \mathbf{u}\mathbf{v}^T\right)$$
$$\mathbf{I} = \mathbf{I} + \mathbf{v}\left(\mathbf{Q}_1^T\mathbf{u}\right)^T + \left(\mathbf{Q}_1^T\mathbf{u}\right)\mathbf{v}^T + \left(\mathbf{u}^T\mathbf{u}\right)\mathbf{v}\mathbf{v}^T$$
$$0 = \mathbf{v}\left(\mathbf{Q}_1^T\mathbf{u}\right)^T + \left(\mathbf{Q}_1^T\mathbf{u}\right)\mathbf{v}^T + \left(\mathbf{u}^T\mathbf{u}\right)\mathbf{v}\mathbf{v}^T$$
$$-\left(\mathbf{u}^T\mathbf{u}\right)\mathbf{v}\mathbf{v}^T = \mathbf{v}\left(\mathbf{u}^T\mathbf{Q}_1\right) + \left(\mathbf{Q}_1^T\mathbf{u}\right)\mathbf{v}^T$$

Right multiplying both sides by $\mathbf{v}$ and using $\|\mathbf{v}\|_2 = 1$, we get:

$$-\left(\mathbf{u}^T\mathbf{u}\right)\mathbf{v} = \left(\mathbf{u}^T\mathbf{Q}_1\mathbf{v}\right)\mathbf{v} + \mathbf{Q}_1^T\mathbf{u}$$
$$\mathbf{Q}_1^T\mathbf{u} = -\left(\mathbf{u}^T\mathbf{u} + \mathbf{u}^T\mathbf{Q}_1\mathbf{v}\right)\mathbf{v} = \lambda\mathbf{v}$$
$$\mathbf{u} = \lambda\mathbf{Q}_1\mathbf{v}, \quad \text{where } \lambda = -\left(\mathbf{u}^T\mathbf{u} + \mathbf{u}^T\mathbf{Q}_1\mathbf{v}\right) \tag{13}$$

Substituting $\mathbf{u}$ using equation (13) in equation (10), we get:

$$\mathbf{Q}_2 - \mathbf{Q}_1 = \lambda\mathbf{Q}_1\mathbf{v}\mathbf{v}^T$$
$$\mathbf{Q}_2 = \mathbf{Q}_1\left(\mathbf{I} + \lambda\mathbf{v}\mathbf{v}^T\right)$$

Since $\mathbf{Q}_2^T\mathbf{Q}_2 = \mathbf{I}$, we have:

$$\mathbf{Q}_2^T\mathbf{Q}_2 = \left(\mathbf{Q}_1\left(\mathbf{I} + \lambda\mathbf{v}\mathbf{v}^T\right)\right)^T\mathbf{Q}_1\left(\mathbf{I} + \lambda\mathbf{v}\mathbf{v}^T\right)$$
$$\mathbf{Q}_2^T\mathbf{Q}_2 = \left(\mathbf{I} + \lambda\mathbf{v}\mathbf{v}^T\right)\mathbf{Q}_1^T\mathbf{Q}_1\left(\mathbf{I} + \lambda\mathbf{v}\mathbf{v}^T\right)$$
$$\mathbf{I} = \left(\mathbf{I} + \lambda\mathbf{v}\mathbf{v}^T\right)\left(\mathbf{I} + \lambda\mathbf{v}\mathbf{v}^T\right)$$
$$\mathbf{I} = \mathbf{I} + 2\lambda\mathbf{v}\mathbf{v}^T + \lambda^2\mathbf{v}\mathbf{v}^T$$
$$\implies \lambda = 0 \text{ or } \lambda = -2$$

Since $\lambda = 0$ would imply $\mathbf{Q}_1 = \mathbf{Q}_2$ which is not allowed by the assumption of the Theorem that $\mathbf{Q}_1 \neq \mathbf{Q}_2$.
$\lambda = -2$ is the only possibility allowed.
This proves the other direction i.e:

$$\mathbf{Q}_2 = \mathbf{Q}_1 \left(\mathbf{I} - 2\mathbf{v}\mathbf{v}^T\right)$$

□

A.2 Proof of Corollary 1

Proof. Subsitute $\mathbf{Q}_1, \mathbf{v}$ as follows in Theorem 1.

$$\mathbf{Q}_1 = \begin{bmatrix} 1 & 0 \\ 0 & 1 \end{bmatrix}$$
$$\mathbf{v} = \begin{bmatrix} +\sin(\theta/2) \\ -\cos(\theta/2) \end{bmatrix}$$
$$\mathbf{Q}_2 = \mathbf{I} - 2\mathbf{v}\mathbf{v}^T$$
$$\mathbf{Q}_2 = \begin{bmatrix} 1 & 0 \\ 0 & 1 \end{bmatrix} - 2 \begin{bmatrix} \sin(\theta/2) \\ -\cos(\theta/2) \end{bmatrix} \begin{bmatrix} \sin(\theta/2) & -\cos(\theta/2) \end{bmatrix}$$
$$\mathbf{Q}_2 = \begin{bmatrix} 1 & 0 \\ 0 & 1 \end{bmatrix} - 2 \begin{bmatrix} \sin^2(\theta/2) & -\sin(\theta/2)\cos(\theta/2) \\ -\sin(\theta/2)\cos(\theta/2) & \cos^2(\theta/2) \end{bmatrix}$$
$$\mathbf{Q}_2 = \begin{bmatrix} 1 - 2\sin^2(\theta/2) & 2\sin(\theta/2)\cos(\theta/2) \\ 2\sin(\theta/2)\cos(\theta/2) & 1 + 2\cos^2(\theta/2) \end{bmatrix}$$
$$\mathbf{Q}_2 = \begin{bmatrix} \cos(\theta) & \sin(\theta) \\ \sin(\theta) & -\cos(\theta) \end{bmatrix}$$

Theorem 1 then directly implies the corollary. □

A.3 Proof of Theorem 2

Proof. We are given the following:

$$\sum_{i=0}^{n-1} (\theta_{2i+1} - \theta_{2i}) = \pi, \qquad \alpha_i = 2\sum_{j=0}^{i} \theta_{i-j}(-1)^j \tag{14}$$

Note that by definition (equation (7)), the function is linear for $\theta_i < \varphi < \theta_{i+1}$ and hence continuous. Furthermore, since $\varphi \in [\theta_0,\ \theta_{2n})$, we proceed to prove continuity for the following two cases:
Case 1: $\theta_i - \epsilon < \varphi < \theta_i + \epsilon, \qquad \epsilon > 0,\ i \geq 1$
Case 2: $\theta_0 < \varphi < \theta_0 + \epsilon, \qquad \theta_{2n} - \epsilon < \varphi < \theta_{2n}, \quad \epsilon > 0$

Proof for Case 1:
Using equation (7), we know that σ_Θ realizes different linear functions for $\theta_i - \epsilon < \varphi < \theta_i$ and $\theta_i < \varphi < \theta_i + \epsilon$.
Thus, for σ_Θ to be continuous, we require that the two linear functions be the same at the boundary i.e $\varphi = \theta_i$.
We first write the input $(z_1,\ z_2)$ in terms of shifted polar coordinates i.e: $(r\cos(\varphi),\ r\sin(\varphi))$ where $r = \sqrt{z_1^2 + z_2^2}$ and $\cos\varphi = z_1/\sqrt{z_1^2 + z_2^2},\ \sin\varphi = z_2/\sqrt{z_1^2 + z_2^2}, \varphi \in [\theta_0, \theta_0 + 2\pi)$
Thus, the function for $\theta_i - \epsilon < \varphi < \theta_i$ is given by:

$$\sigma_\Theta(r\cos\varphi, r\sin\varphi) = \begin{bmatrix} \cos\alpha_{i-1} & \sin\alpha_{i-1} \\ (-1)^{i-1}\sin\alpha_{i-1} & (-1)^i\cos\alpha_{i-1} \end{bmatrix} \begin{bmatrix} r\cos\varphi \\ r\sin\varphi \end{bmatrix} \tag{15}$$

Similarly, the function for $\theta_i < \varphi < \theta_i + \epsilon$ is given by:

$$\sigma_\Theta(r\cos\varphi, r\sin\varphi) = \begin{bmatrix} \cos\alpha_i & \sin\alpha_i \\ (-1)^i\sin\alpha_i & (-1)^{i+1}\cos\alpha_i \end{bmatrix} \begin{bmatrix} r\cos\varphi \\ r\sin\varphi \end{bmatrix} \tag{16}$$

The difference in the function values at the boundary i.e $\varphi = \theta_i$, obtained by subtracting equations (16) and (15) is given as follows:

$$\begin{bmatrix} \cos\alpha_i & \sin\alpha_i \\ (-1)^i \sin\alpha_i & (-1)^{i+1}\cos\alpha_i \end{bmatrix} \begin{bmatrix} r\cos\theta_i \\ r\sin\theta_i \end{bmatrix} - \begin{bmatrix} \cos\alpha_{i-1} & \sin\alpha_{i-1} \\ (-1)^{i-1}\sin\alpha_{i-1} & (-1)^i\cos\alpha_{i-1} \end{bmatrix} \begin{bmatrix} r\cos\theta_i \\ r\sin\theta_i \end{bmatrix}$$

$$= r \begin{bmatrix} \cos\alpha_i - \cos\alpha_{i-1} & \sin\alpha_i - \sin\alpha_{i-1} \\ (-1)^i\sin\alpha_i - (-1)^{i-1}\sin\alpha_{i-1} & (-1)^{i+1}\cos\alpha_i - (-1)^i\cos\alpha_{i-1} \end{bmatrix} \begin{bmatrix} \cos\theta_i \\ \sin\theta_i \end{bmatrix}$$

$$= r \begin{bmatrix} \cos\alpha_i - \cos\alpha_{i-1} & \sin\alpha_i - \sin\alpha_{i-1} \\ (-1)^i(\sin\alpha_i + \sin\alpha_{i-1}) & (-1)^{i+1}(\cos\alpha_i + \cos\alpha_{i-1}) \end{bmatrix} \begin{bmatrix} \cos\theta_i \\ \sin\theta_i \end{bmatrix}$$

Using sum-to-product trigonometric identities, the above equals:

$$= r \begin{bmatrix} 2\sin\left(\frac{\alpha_{i-1}-\alpha_i}{2}\right)\sin\left(\frac{\alpha_{i-1}+\alpha_i}{2}\right) & 2\sin\left(\frac{\alpha_i-\alpha_{i-1}}{2}\right)\cos\left(\frac{\alpha_i+\alpha_{i-1}}{2}\right) \\ 2(-1)^i\sin\left(\frac{\alpha_i+\alpha_{i-1}}{2}\right)\cos\left(\frac{\alpha_i-\alpha_{i-1}}{2}\right) & 2(-1)^{i+1}\cos\left(\frac{\alpha_{i-1}-\alpha_i}{2}\right)\cos\left(\frac{\alpha_{i-1}+\alpha_i}{2}\right) \end{bmatrix} \begin{bmatrix} \cos\theta_i \\ \sin\theta_i \end{bmatrix}$$

$$= 2r \begin{bmatrix} \sin\left(\frac{\alpha_{i-1}-\alpha_i}{2}\right)\sin\left(\frac{\alpha_{i-1}+\alpha_i}{2}\right) & -\sin\left(\frac{\alpha_{i-1}-\alpha_i}{2}\right)\cos\left(\frac{\alpha_i+\alpha_{i-1}}{2}\right) \\ (-1)^i\sin\left(\frac{\alpha_i+\alpha_{i-1}}{2}\right)\cos\left(\frac{\alpha_i-\alpha_{i-1}}{2}\right) & (-1)^{i+1}\cos\left(\frac{\alpha_{i-1}-\alpha_i}{2}\right)\cos\left(\frac{\alpha_{i-1}+\alpha_i}{2}\right) \end{bmatrix} \begin{bmatrix} \cos\theta_i \\ \sin\theta_i \end{bmatrix}$$

$$= 2r \begin{bmatrix} \sin\left(\frac{\alpha_{i-1}-\alpha_i}{2}\right) \\ (-1)^i\cos\left(\frac{\alpha_{i-1}-\alpha_i}{2}\right) \end{bmatrix} \begin{bmatrix} \sin\left(\frac{\alpha_{i-1}+\alpha_i}{2}\right) & -\cos\left(\frac{\alpha_{i-1}+\alpha_i}{2}\right) \end{bmatrix} \begin{bmatrix} \cos\theta_i \\ \sin\theta_i \end{bmatrix}$$

Using equation (14), we directly have: $\alpha_i = 2\theta_i - \alpha_{i-1}$. Thus, the above equation reduces to:

$$= 2r \begin{bmatrix} \sin(\theta_i - \alpha_i) \\ (-1)^i\cos(\theta_i - \alpha_i) \end{bmatrix} \begin{bmatrix} \sin(\theta_i) & -\cos(\theta_i) \end{bmatrix} \begin{bmatrix} \cos\theta_i \\ \sin\theta_i \end{bmatrix} = \begin{bmatrix} 0. \\ 0. \end{bmatrix}$$

Hence, the linear functions given by equations (15) and (16) are equal at $\varphi = \theta_i$. This proves that the function is continuous for Case 1.

Proof for Case 2:
Using equation (7), we know that σ_Θ realizes different linear functions for $\theta_0 < \varphi < \theta_0 + \epsilon$ and $\theta_{2n} - \epsilon < \varphi < \theta_{2n}$.
Thus, for σ_Θ to be continuous, we require that the two linear functions be the same at the boundary i.e $\varphi = \theta_0$.
As before, we first write the input $(z_1,\ z_2)$ in terms of shifted polar coordinates i.e: $(r\cos(\varphi),\ r\sin(\varphi))$.
Thus, the function for $\theta_0 < \varphi < \theta_0 + \epsilon$ is given by:

$$\sigma_\Theta(r\cos\varphi, r\sin\varphi) = \begin{bmatrix} \cos\alpha_0 & \sin\alpha_0 \\ \sin\alpha_0 & -\cos\alpha_0 \end{bmatrix} \begin{bmatrix} r\cos\varphi \\ r\sin\varphi \end{bmatrix} \tag{17}$$

Similarly, the function for $\theta_{2n} - \epsilon < \phi < \theta_{2n}$ is given by:

$$\sigma_\Theta(r\cos\varphi, r\sin\varphi) = \begin{bmatrix} \cos\alpha_{2n-1} & \sin\alpha_{2n-1} \\ (-1)^i\sin\alpha_{2n-1} & (-1)^{i+1}\cos\alpha_{2n-1} \end{bmatrix} \begin{bmatrix} r\cos\varphi \\ r\sin\varphi \end{bmatrix} \tag{18}$$

Using equation (14), α_{2n-1} is given as follows:

$$\alpha_{2n-1} = 2\sum_{i=0}^{2n-1} \theta_{2n-1-i}(-1)^i = 2\sum_{i=0}^{n-1}(\theta_{2i+1} - \theta_{2i}) = 2\pi$$

Thus, equation (18) reduces to:

$$\sigma_\Theta(r\cos\varphi, r\sin\varphi) = \begin{bmatrix} 1 & 0 \\ 0 & 1 \end{bmatrix} \begin{bmatrix} r\cos\varphi \\ r\sin\varphi \end{bmatrix} \tag{19}$$

The difference in the function values at the boundary i.e $\varphi = \theta_0$, obtained by subtracting equations (19) and (17) is given as follows:

$$\begin{bmatrix} 1 & 0 \\ 0 & 1 \end{bmatrix} \begin{bmatrix} r\cos\theta_0 \\ r\sin\theta_0 \end{bmatrix} - \begin{bmatrix} \cos\alpha_0 & \sin\alpha_0 \\ \sin\alpha_0 & -\cos\alpha_0 \end{bmatrix} \begin{bmatrix} r\cos\theta_0 \\ r\sin\theta_0 \end{bmatrix}$$

$$= r \begin{bmatrix} 1-\cos\alpha_0 & -\sin\alpha_0 \\ -\sin\alpha_0 & 1+\cos\alpha_0 \end{bmatrix} \begin{bmatrix} \cos\theta_0 \\ \sin\theta_0 \end{bmatrix}$$

Using the trigonometric identities: $1 - \cos(\theta) = 2\sin^2(\theta/2)$, $1 + \cos(\theta) = 2\cos^2(\theta/2)$ and $\sin(\theta) = 2\sin(\theta/2)\cos(\theta/2)$, we have:

$$= r \begin{bmatrix} 2\sin^2(\frac{\alpha_0}{2}) & -2\sin(\frac{\alpha_0}{2})\cos(\frac{\alpha_0}{2}) \\ -2\sin(\frac{\alpha_0}{2})\cos(\frac{\alpha_0}{2}) & 2\cos^2(\frac{\alpha_0}{2}) \end{bmatrix} \begin{bmatrix} \cos\theta_0 \\ \sin\theta_0 \end{bmatrix}$$
$$= 2r \begin{bmatrix} \sin(\frac{\alpha_0}{2}) \\ -\cos(\frac{\alpha_0}{2}) \end{bmatrix} \begin{bmatrix} \sin(\frac{\alpha_0}{2}) & -\cos(\frac{\alpha_0}{2}) \end{bmatrix} \begin{bmatrix} \cos\theta_0 \\ \sin\theta_0 \end{bmatrix}$$

Using equation (14), we have: $\alpha_0 = 2\theta_0$. Thus, the above equation reduces to:

$$= 2r \begin{bmatrix} \sin(\theta_0) \\ -\cos(\theta_0) \end{bmatrix} \begin{bmatrix} \sin(\theta_0) & -\cos(\theta_0) \end{bmatrix} \begin{bmatrix} \cos\theta_0 \\ \sin\theta_0 \end{bmatrix} = \begin{bmatrix} 0. \\ 0. \end{bmatrix}$$

Hence, the linear functions given by equations (17) and (19) are equal at $\varphi = \theta_0$.
This proves that the function is continuous for Case 2. □

A.4 Proof of Theorem 3

Proof. We proceed by computing the Lipschitz constant of the function $f_l - f_i$.
The gradient of the function: $f_l - f_i$ at $\mathbf{x}$ can be computed using the chain rule:

$$\nabla_{\mathbf{x}} (f_l - f_i) = (\mathbf{W}_{l,:} - \mathbf{W}_{i,:})^T \nabla_{\mathbf{x}} g$$

Since g is given to be 1-Lipschitz, the Lipschitz constant of $f_l - f_i$ can be computed using the above equation as follows:

$$\|\nabla_{\mathbf{x}} (f_l - f_i)\|_2 \leq \| (\mathbf{W}_{l,:} - \mathbf{W}_{i,:})^T (\nabla_{\mathbf{x}} g) \|_2$$
$$\|\nabla_{\mathbf{x}} (f_l - f_i)\|_2 \leq \|\mathbf{W}_{l,:} - \mathbf{W}_{i,:}\|_2 \|\nabla_{\mathbf{x}} g\|_2 \leq \|\mathbf{W}_{l,:} - \mathbf{W}_{i,:}\|_2$$

Thus, the distance of $\mathbf{x}$ to the decision boundary $f_l - f_i = 0$, is lower bounded by:

$$\min_{f_l(\mathbf{x}^*) = f_i(\mathbf{x}^*)} \|\mathbf{x}^* - \mathbf{x}\|_2 \geq \frac{f_l(\mathbf{x}) - f_i(\mathbf{x})}{\|\mathbf{W}_{l,:} - \mathbf{W}_{i,:}\|_2}$$

Thus, the distance to decision boundary across all classes $i \neq l$ is lower bounded by:

$$\min_{i \neq l} \min_{f_l(\mathbf{x}^*) = f_i(\mathbf{x}^*)} \|\mathbf{x}^* - \mathbf{x}\|_2 \geq \min_{i \neq l} \frac{f_l(\mathbf{x}) - f_i(\mathbf{x})}{\|\mathbf{W}_{l,:} - \mathbf{W}_{i,:}\|_2}$$

□

B Verification that $\sigma_\theta(z_1, z_2)$ always lies on one side of the hyperplane

Consider the case: $z_1 \sin(\theta/2) - z_2 \cos(\theta/2) > 0$
In this case $\sigma_\theta(z_1, z_2) = (z_1, z_2)$ and the result follows directly.
Consider the other case: $z_1 \sin(\theta/2) - z_2 \cos(\theta/2) \leq 0$

$$\begin{bmatrix} a_1 \\ a_2 \end{bmatrix} = \begin{bmatrix} \cos\theta & \sin\theta \\ \sin\theta & -\cos\theta \end{bmatrix} \begin{bmatrix} z_1 \\ z_2 \end{bmatrix} = \begin{bmatrix} z_1\cos\theta + z_2\sin\theta \\ z_1\sin\theta - z_2\cos\theta \end{bmatrix}$$
$$a_1 \sin(\theta/2) - a_2 \cos(\theta/2) = (z_1\cos\theta + z_2\sin\theta)\sin(\theta/2) - (z_1\sin\theta - z_2\cos\theta)\cos(\theta/2)$$
$$= z_1(\cos\theta\sin(\theta/2) - \sin\theta\cos(\theta/2)) + z_2(\sin\theta\sin(\theta/2) + \cos\theta\cos(\theta/2))$$
$$= -z_1\sin(\theta/2) + z_2\cos(\theta/2)$$

Since $z_1 \sin(\theta/2) - z_2 \cos(\theta/2) \leq 0$, we have $-z_1 \sin(\theta/2) + z_2 \cos(\theta/2) \geq 0$.

C Higher order Householder activation functions

We know that $\mathrm{MaxMin}(z_1, z_2) = (\max(z_1, z_2), \min(z_1, z_2))$ where $z_1, z_2 \in \mathbb{R}$. Because $\max(z_1, z_2) > \min(z_1, z_2)$, applying MaxMin again gives the same result i.e $\mathrm{MaxMin} \circ \mathrm{MaxMin} =$

MaxMin. Now consider the function σ_θ (discussed in the maintext, given below for convenience):

$$\sigma_\theta\left(z_1, z_2\right) = \begin{cases} \begin{bmatrix} 1 & 0 \\ 0 & 1 \end{bmatrix} \begin{bmatrix} z_1 \\ z_2 \end{bmatrix} & \text{if } \; z_1 \sin\left(\theta/2\right) - z_2 \cos\left(\theta/2\right) > 0 \\ \begin{bmatrix} \cos\theta & \sin\theta \\ \sin\theta & -\cos\theta \end{bmatrix} \begin{bmatrix} z_1 \\ z_2 \end{bmatrix} & \text{if } \; z_1 \sin\left(\theta/2\right) - z_2 \cos\left(\theta/2\right) \leq 0 \end{cases}$$

From Figure 1, we observe that if $(u_1, u_2) = \sigma_\theta(z_1, z_2)$, then (u_1, u_2) always lies on the right side of the hyperplane (pink colored region). In other words, $u_1 \sin\left(\theta/2\right) - u_2 \cos\left(\theta/2\right) > 0 \;\; \forall \; z_1, z_2$ (proof in Appendix B). This further implies that $\sigma_\theta \circ \sigma_\theta = \sigma_\theta$.

However from Figure 2a in the maintext, we observe that if we use a different angle ϕ where $\phi \neq \theta + 2n\pi$ for some $n \in \mathbb{Z}$, then $\sigma_\phi(u_1, u_2) \neq (u_1, u_2)$ for all (u_1, u_2) in the pink colored region ($u_1 \sin\left(\theta/2\right) - u_2 \cos\left(\theta/2\right) > 0$). This motivates us to construct the function $\sigma^{(n)} : \mathbb{R}^2 \to \mathbb{R}^2$ defined as follows:

$$\sigma^{(n)} = \underbrace{\sigma_\theta \circ \sigma_\theta \circ \sigma_\theta \ldots \circ \sigma_\theta}_{n \text{ times, } \theta\text{'s can be different}} \tag{20}$$

Clearly, $\sigma^{(n)}$ has a larger number of linear regions than σ_θ and thus expected to have more expressive power. However, a drawback of using $\sigma^{(n)}$ is that it requires a sequential application of σ_θ which can be expensive if the number of iterations n is large. To address this limitation, first observe that σ_θ realizes the same linear function for (z_1, z_2) and (cz_1, cz_2) when $c > 0$ i.e $\nabla_{(z_1, z_2)}\, \sigma_\theta = \nabla_{(cz_1, cz_2)}\, \sigma_\theta$. Since σ_θ is piecewise linear, $\sigma_\theta(cz_1, cz_2) = c\sigma_\theta(z_1, z_2)$. Thus, the input of the next function in the iteration is scaled by c as well and its linear function (or the Jacobian) remains unchanged. By induction, same holds for all the subsequent iterations. By chain rule, the Jacobian of composition of functions is equal to the product of Jacobian of each individual function. Since the Jacobian of each function is unchanged on scaling by $c > 0$, the Jacobian $\nabla_{(z_1, z_2)}\, \sigma^{(n)}$ also remains unchanged: $\nabla_{(z_1, z_2)}\, \sigma^{(n)} = \nabla_{(cz_1, cz_2)}\, \sigma^{(n)}$. This suggests that it is possible to determine the Jacobian $\nabla_{(z_1, z_2)}\, \sigma^{(n)}$ for the input (z_1, z_2) by first converting to the polar coordinates $(\sqrt{z_1^2 + z_2^2},\; \varphi)$ and then using the phase angle φ alone (where $\cos(\varphi) = z_1/\sqrt{z_1^2 + z_2^2},\; \sin(\varphi) = z_2/\sqrt{z_1^2 + z_2^2}$).

This motivates us to construct another GNP piecewise linear activation that only depends on the phase of the input but unlike σ_θ, it is allowed to have more than 2 linear regions without requiring a sequential application. This construction is given in the following theorem (example in maintext Figure 2b):

Theorem 2. *Given:* $0 \leq \theta_0 < \theta_1 \cdots < \theta_{2n} = 2\pi + \theta_0$ *such that* $\sum_{i=0}^{n-1}(\theta_{2i+1} - \theta_{2i}) = \pi$ *and* $\alpha_i = 2\sum_{j=0}^{i} \theta_{i-j}(-1)^j$*, The function* $\sigma_\Theta : \mathbb{R}^2 \to \mathbb{R}^2$ *is continuous, GNP and* 1*-Lipschitz where* $\Theta = [\theta_0, \theta_1, \ldots, \theta_{2n-1}]$ *(also called Householder Activation of order* n *in* 2 *dimensions):*

$$\sigma_\Theta(z_1, z_2) = \begin{bmatrix} \cos\alpha_i & \sin\alpha_i \\ (-1)^i \sin\alpha_i & (-1)^{i+1}\cos\alpha_i \end{bmatrix} \begin{bmatrix} z_1 \\ z_2 \end{bmatrix} \qquad \theta_i \leq \varphi < \theta_{i+1}$$

where $\varphi \in [\theta_0,\; \theta_{2n} = 2\pi + \theta_0)$ *and* $\cos(\varphi) = z_1/\sqrt{z_1^2 + z_2^2},\;\; \sin(\varphi) = z_2/\sqrt{z_1^2 + z_2^2}$.

Using the definition of α_i, α_{2n-1} can be computed as follows:

$$\alpha_{2n-1} = 2\sum_{j=0}^{2n-1} \theta_{2n-1-j}(-1)^j = 2\sum_{j=0}^{n-1}(\theta_{2n-1-2j} - \theta_{2n-2-2j}) = 2\sum_{j=0}^{n-1}(\theta_{2j+1} - \theta_{2j}) = 2\pi$$

$$\sigma_\Theta(z_1, z_2) = \begin{bmatrix} \cos\alpha_{2n-1} & \sin\alpha_{2n-1} \\ -\sin\alpha_{2n-1} & \cos\alpha_{2n-1} \end{bmatrix} \begin{bmatrix} z_1 \\ z_2 \end{bmatrix} = (z_1, z_2) \qquad \theta_{2n-1} \leq \varphi < \theta_{2n} (= \theta_0 + 2\pi)$$

By continuity, $\sigma_\Theta(z_1, z_2) = (z_1, z_2)$ for $\varphi = \theta_0$. Thus if we set $\theta_0 = 0$, σ_Θ is fixed to be identity when $\varphi = 0$ (or $z_2 = 0$). However, a learnable θ_0 offers the flexibility of choosing arbitrary intervals around the $\varphi = \theta_0$ to be the identity function (while of course allowing $\theta_0 = 0$). Since we can choose any interval of 2π for the phase angle, we choose $\varphi \in [\theta_0,\; \theta_{2n} = \theta_0 + 2\pi)$ instead of the usual $[0,\; 2\pi)$ to allow this possibility. We call $(\sqrt{z_1^2 + z_2^2},\; \varphi)$, the *shifted polar coordinates*.

Additionally, we make the following observations about Theorem 2. First, by construction σ_Θ has $2n$ linear regions. Second, since $\sum_{i=0}^{n-1}(\theta_{2i+1} - \theta_{2i}) = \pi$, the sum of angles subtended by linear regions with determinant -1 equals π. This in turn implies that sum of angles subtended by linear regions with determinant $+1$ must also equal π. Third, again using $\sum_{j=0}^{n-1}(\theta_{2j+1} - \theta_{2j}) = \pi$, we know that only $2n-1$ of the $2n$ parameters in $[\theta_0,\ \theta_1,\ \theta_2,\ \ldots,\ \theta_{2n-1}]$ can be chosen independently implying that σ_Θ has $2n-1$ learnable parameters. In contrast, $\sigma^{(n)}$ has only n learnable parameters. Fourth, when $n = 1$, σ_Θ reduces to the original σ_θ activation.

Because every function of the form $\sigma^{(n)}$ (equation (20)) can have potentially 2^n linear regions, while σ_Θ has only $2n$ linear regions, σ_Θ cannot express every function of the form $\sigma^{(n)}$. The primary benefit of using σ_Θ is that it can be easily applied by first determining the angle φ (using shifted polar coordinates), the region $[\theta_i, \theta_{i+1})$ to which φ belongs and the Jacobian for this region. This requires 1 multiplication with the Jacobian instead of n required for $\sigma^{(n)}$.

D Extension to higher dimensions

We introduced Householder activation function of Order 1 in m dimensions in maintext Definition 1. However, it suffers from the limitation that it has only 2 linear regions thus limiting its expressive power. The construction given in Appendix Section C allows more than 2 linear regions but is valid only for 2 dimensional inputs. This motivates us to construct Householder activations that depend on all the m components of input $\mathbf{z} \in \mathbb{R}^m,\ (m \geq 3)$ while allowing for more than 2 linear regions.

A straightforward way of constructing such an activation function is to apply an orthogonal matrix $\mathbf{Q} \in \mathbb{R}^{m\times m}$, followed by dividing the output $\mathbf{Qz}$ into groups of size 2 each and then applying σ_θ to each group. However, since 1-Lipschitz neural networks involve multiplication with an orthogonal weight matrix followed by GNP activation anyway, this construction is trivial because it does not lead to additional gains in expressive power over using 2 dimensional σ_Θ activation functions.

Recall that the function $\sigma_\mathbf{v}$ is given by the following equation:

$$\sigma_\mathbf{v}(\mathbf{z}) = \begin{cases} \mathbf{z}, & \mathbf{v}^T\mathbf{z} > 0, \\ (\mathbf{I} - 2\mathbf{v}\mathbf{v}^T)\mathbf{z}, & \mathbf{v}^T\mathbf{z} \leq 0. \end{cases} \tag{21}$$

By a similar analysis as for the 2-dimensional case (Figure 2 in maintext), a repeated application of $\sigma_\mathbf{v}$ leads to increased number of linear regions and thus higher expressive power. This motivates us to construct the function $\sigma^{(m,n)} : \mathbb{R}^m \to \mathbb{R}^m$ by applying the function $\sigma_\mathbf{v}$ (equation (21)) n times iteratively with different learnable parameter $\mathbf{v}$ at each iteration:

$$\sigma^{(m,n)} = \underbrace{\sigma_\mathbf{v} \circ \sigma_\mathbf{v} \circ \sigma_\mathbf{v} \ldots \circ \sigma_\mathbf{v}}_{n \text{ times, } \mathbf{v}\text{'s can be different}}$$

Since $\sigma_\mathbf{v}$ realizes the same linear function for both the inputs $\mathbf{z}$ and $c\mathbf{z}$ i.e $\nabla_\mathbf{z}\, \sigma_\mathbf{v} = \nabla_{c\mathbf{z}}\, \sigma_\mathbf{v}$ when $c > 0$, $\sigma^{(m,n)}$ satisfies this property as well. This suggests that it is possible to determine the Jacobian of $\sigma^{(m,n)}$ for the given input $\mathbf{z}$ by projecting $\mathbf{z}$ onto a unit sphere: $\mathbf{z}/\|\mathbf{z}\|_2$. Moreover, we want our constructed function to have at least $2n$ linear regions while requiring k iterations of $\sigma_\mathbf{v}$ where k is independent of n. This motivates the following open question:

Open Problem. *Can non-trivial order-n ($n > 1$) householder activation functions with $2n$ linear regions be constructed for m dimensional input ($m > 2$) using k iterations of $\sigma_\mathbf{v}$ where k is independent of n (but may depend on m)?*

E Additional results on CIFAR-10

The rows "BCOP", "Cayley" and "SOC (baseline)" all use the MaxMin activation function. "SOC + HH" replaces MaxMin with 2D Householder activation of order 1 (σ_θ), "+ CR" adds Certificate Regularization (CR) with $\gamma = 0.1$ (while using σ_θ as the activation function).

In Table 6, the row "SOC + $\mathrm{HH}^{(2)}$" uses Householder activation of order 2 (σ_Θ defined in Theorem 2), "+ CR" adds Certificate Regularization (CR) with $\gamma = 0.1$ (while using the HH activation of order 2 i.e σ_Θ as the activation function).

None of the results in Tables 4, 5 and 6 include Last Layer Normalization (LLN).

Architecture	Running times (seconds)	
	MaxMin	**HH**
LipConvnet-5	3.7864	3.86
LipConvnet-10	5.3677	5.6014
LipConvnet-15	7.234	7.3503
LipConvnet-20	9.536	9.3753
LipConvnet-25	11.0512	11.2692
LipConvnet-30	12.5135	13.6866
LipConvnet-35	14.5539	15.0921
LipConvnet-40	17.1907	17.1928

Table 3: Inference times for various networks on the complete test dataset of CIFAR-10 with 10000 samples. None of these networks include Last Layer Normalization (LLN).

Architecture	**Methods**	**Standard Accuracy**	**Provable Robust Acc.** ($\rho =$)			**Increase**
			36/255	72/255	108/255	(108/255)
LipConvnet-5	BCOP	74.25%	58.01%	40.34%	25.21%	-1.88%
	Cayley	72.37%	55.92%	38.65%	24.27%	-2.82%
	SOC (baseline)	75.78%	59.18%	42.01%	27.09%	(+0%)
	SOC + HH	**76.30%**	60.12%	43.20%	27.39%	+0.30%
	+ CR	75.31%	**60.37%**	**45.62%**	**32.38%**	**+5.29%**
LipConvnet-10	BCOP	74.47%	58.48%	40.77%	26.16%	-2.99%
	Cayley	74.30%	57.99%	40.75%	25.93%	-3.22%
	SOC (baseline)	76.45%	60.86%	44.15%	29.15%	(+0%)
	SOC + HH	**76.86%**	61.52%	44.91%	29.90%	+0.75%
	+ CR	76.23%	**62.57%**	**47.70%**	**34.15%**	**+5.00%**
LipConvnet-15	BCOP	73.86%	57.39%	39.33%	24.86%	-4.80%
	Cayley	71.92%	54.55%	37.67%	23.50%	-6.16%
	SOC (baseline)	76.68%	61.36%	44.28%	29.66%	(+0%)
	SOC + HH	**77.41%**	61.92%	45.60%	31.10%	+1.44%
	+ CR	76.39%	**62.96%**	**48.47%**	**35.47%**	**+5.81%**
LipConvnet-20	BCOP	69.84%	52.10%	34.75%	21.09%	-9.99%
	Cayley	68.87%	51.88%	35.56%	21.72%	-9.36%
	SOC (baseline)	**76.90%**	61.87%	45.79%	31.08%	(+0%)
	SOC + HH	76.99%	61.76%	45.59%	30.99%	-0.09%
	+ CR	76.34%	**62.63%**	**48.69%**	**36.04%**	**+4.96%**

Table 4: Results for provable robustness on the CIFAR-10 dataset using shallow networks. None of these results include Last Layer Normalization (LLN).

Architecture	Methods	Standard Accuracy	Provable Robust Acc. ($\rho =$)			Increase
			36/255	72/255	108/255	(108/255)
LipConvnet-25	BCOP	68.47%	49.92%	31.99%	18.62%	-9.98%
	Cayley	64.00%	45.55%	29.24%	16.99%	-11.61%
	SOC (baseline)	75.24%	60.17%	43.55%	28.60%	(+0%)
	SOC + HH	**76.37%**	61.50%	44.72%	29.83%	+1.23%
	+ CR	75.21%	**61.98%**	**47.93%**	**34.92%**	**+6.32%**
LipConvnet-30	BCOP	64.11%	43.39%	25.02%	12.15%	-15.90%
	Cayley	58.83%	38.68%	22.07%	10.68%	-17.37%
	SOC (baseline)	74.51%	59.06%	42.46%	28.05%	(+0%)
	SOC + HH	**75.25%**	59.90%	43.85%	29.35%	+1.30%
	+ CR	74.23%	**60.64%**	**46.51%**	**34.08%**	**+6.03%**
LipConvnet-35	BCOP	63.05%	41.71%	23.30%	11.36%	-15.84%
	Cayley	53.55%	32.37%	16.18%	6.33%	-20.87%
	SOC (baseline)	73.73%	58.50%	41.75%	27.20%	(+0%)
	SOC + HH	**75.44%**	61.05%	45.38%	30.85%	+3.65%
	+ CR	74.25%	**61.30%**	**47.60%**	**35.21%**	**+8.01%**
LipConvnet-40	BCOP	60.17%	38.86%	21.20%	9.08%	-15.05%
	Cayley	51.26%	27.90%	12.06%	3.81%	-20.32%
	SOC (baseline)	71.63%	54.39%	37.92%	24.13%	(+0%)
	SOC + HH	**73.24%**	58.12%	42.24%	28.48%	+4.35%
	+ CR	72.59%	**59.04%**	**44.92%**	**32.87%**	**+8.74%**

Table 5: Results for provable robustness against adversarial examples on the CIFAR-10 dataset. None of these results include Last Layer Normalization (LLN).

Architecture	Methods	Standard Accuracy	Provable Robust Acc. ($\rho =$)			Increase
			36/255	72/255	108/255	(108/255)
LipConvnet-5	**SOC + HH$^{(2)}$**	75.85%	59.66%	42.68%	27.44%	+0.35%
	+ CR	74.85%	60.56%	44.96%	31.98%	+4.59%
LipConvnet-10	**SOC + HH$^{(2)}$**	76.80%	61.44%	44.91%	29.70%	+0.55%
	+ CR	76.30%	62.11%	47.85%	34.49%	+5.34%
LipConvnet-15	**SOC + HH$^{(2)}$**	77.41%	62.21%	45.11%	30.49%	+0.83%
	+ CR	75.73%	62.21%	47.92%	35.26%	+5.60%
LipConvnet-20	**SOC + HH$^{(2)}$**	76.69%	61.58%	45.39%	30.89%	-0.19%
	+ CR	75.72%	62.61%	48.30%	35.29%	+4.21%
LipConvnet-25	**SOC + HH$^{(2)}$**	76.12%	61.24%	44.81%	29.63%	+1.03%
	+ CR	75.38%	61.94%	47.67%	34.22%	+5.62%
LipConvnet-30	**SOC + HH$^{(2)}$**	75.09%	60.01%	44.22%	29.39%	+1.34%
	+ CR	74.88%	61.23%	46.63%	34.02%	+5.97%
LipConvnet-35	**SOC + HH$^{(2)}$**	73.93%	58.61%	42.29%	28.47%	+1.27%
	+ CR	74.14%	60.72%	46.67%	34.64%	+7.44%
LipConvnet-40	**SOC + HH$^{(2)}$**	70.90%	54.96%	38.94%	24.90%	+0.77%
	+ CR	72.28%	57.67%	43.00%	30.66%	+6.53%

Table 6: Results for provable robustness on CIFAR-10 using HH activation of Order 2 (σ_{Θ}).
Increase (108/255) is calculated with respect to SOC baseline (from Tables 4, 5).
None of these results include Last Layer Normalization (LLN).

Architecture	Methods	Standard Accuracy	Provable Robust Acc. ($\rho =$)			Increase
			(36/255)	(72/255)	(108/255)	(Standard)
LipConvnet-5	SOC (no LLN)	75.78%	59.18%	42.01%	27.09%	(+0%)
	SOC + LLN	**75.78%**	**59.58%**	**42.45%**	**27.20%**	**+0.00%**
LipConvnet-10	SOC (no LLN)	76.45%	60.86%	44.15%	29.15%	(+0%)
	SOC + LLN	**76.69%**	**61.08%**	**44.04%**	**29.19%**	**+0.24%**
LipConvnet-15	SOC (no LLN)	76.68%	61.36%	44.28%	29.66%	(+0%)
	SOC + LLN	**76.84%**	**61.94%**	**45.51%**	**30.28%**	**+0.16%**
LipConvnet-20	SOC (no LLN)	**77.05%**	**61.87%**	**45.79%**	**31.08%**	**(+0%)**
	SOC + LLN	76.71%	61.44%	44.92%	30.19%	-0.34%
LipConvnet-25	SOC (no LLN)	75.24%	60.17%	43.55%	28.60%	(+0%)
	SOC + LLN	**76.54%**	**61.21%**	**44.18%**	**29.47%**	**+1.30%**
LipConvnet-30	SOC (no LLN)	**74.51%**	**59.06%**	**42.46%**	**28.05%**	**(+0%)**
	SOC + LLN	74.26%	58.97%	41.82%	26.93%	-0.25%
LipConvnet-35	SOC (no LLN)	73.73%	58.50%	41.75%	27.20%	(+0%)
	SOC + LLN	**74.32%**	**59.05%**	**42.34%**	**28.14%**	**+0.59%**
LipConvnet-40	SOC (no LLN)	71.63%	54.39%	37.92%	24.13%	(+0%)
	SOC + LLN	**74.03%**	**58.27%**	**41.75%**	**27.12%**	**+2.40%**

Table 7: Results for provable robustness on the CIFAR-10 dataset with and without LLN

F Additional Results on CIFAR-100

All results in Tables 10, 11 and 12 include Last Layer Normalization (LLN).

The rows "BCOP", "Cayley" and "SOC (baseline)" all use the MaxMin activation function. "SOC + HH" replaces MaxMin with 2D Householder activation of order 1 (σ_θ), "+ CR" adds Certificate Regularization (CR) with $\gamma = 0.1$ (while using σ_θ as the activation function).

In Table 12, the row "SOC + $\mathrm{HH}^{(2)}$" uses Householder activation of order 2 (σ_Θ defined in Theorem 2), "+ CR" adds Certificate Regularization (CR) with $\gamma = 0.1$ (while using the HH activation of order 2 i.e σ_Θ as the activation function).

Architecture	**Methods**	**Standard Accuracy**	**Provable Robust Acc.** ($\rho =$)			**Increase**
			36/255	72/255	108/255	(Standard)
LipConvnet-5	SOC + MaxMin	42.71%	27.86%	17.45%	9.99%	_
	+ LLN	45.86%	31.93%	21.17%	13.21%	+3.15%
	+ HH	**46.36%**	32.64%	21.19%	13.12%	**+3.65%**
	+ CR	45.82%	**32.99%**	**22.48%**	**14.79%**	+3.11%
LipConvnet-10	SOC + MaxMin	43.72%	29.39%	18.56%	11.16%	_
	+ LLN	46.88%	33.32%	22.08%	13.87%	+3.16%
	+ HH	**47.96%**	34.30%	22.35%	14.48%	**+4.24%**
	+ CR	47.07%	**34.53%**	**23.50%**	**15.66%**	+3.35%

Table 8: Results for provable robustness against adversarial examples on the CIFAR-100 dataset.

Architecture	**Running times (in seconds)**		
	MaxMin (no LLN)	**MaxMin (LLN)**	**HH (LLN)**
LipConvnet-5	3.7568	3.5002	3.6673
LipConvnet-10	5.3714	5.5482	5.5533
LipConvnet-15	7.3092	7.2595	7.3127
LipConvnet-20	9.005	9.2043	9.308
LipConvnet-25	10.9321	10.7868	11.726
LipConvnet-30	12.3198	13.2168	13.6275
LipConvnet-35	14.427	14.575	15.7069
LipConvnet-40	16.0911	16.2535	17.1015

Table 9: Inference times for various networks on the CIFAR-100 test dataset. Similar to CIFAR-10 (in Table 3), these numbers are for the whole test dataset with 10000 samples.

Architecture	Methods	Standard Accuracy	Provable Robust Acc. ($\rho =$)			Increase
			36/255	72/255	108/255	(108/255)
LipConvnet-5	BCOP	46.31%	31.55%	20.34%	12.52%	-0.69%
	Cayley	44.61%	31.01%	19.84%	12.43%	-0.78%
	SOC (baseline)	45.86%	31.93%	21.17%	13.21%	(+0%)
	SOC + HH	**46.36%**	32.64%	21.19%	13.12%	-0.09%
	+ CR	45.82%	**32.99%**	**22.48%**	**14.79%**	**+1.58%**
LipConvnet-10	BCOP	45.36%	31.71%	20.48%	12.40%	-1.47%
	Cayley	45.79%	31.91%	20.69%	12.78%	-1.09%
	SOC (baseline)	46.88%	33.32%	22.08%	13.87%	(+0%)
	SOC + HH	**47.96%**	34.30%	22.35%	14.48%	+0.61%
	+ CR	47.07%	**34.53%**	**23.50%**	**15.66%**	**+1.79%**
LipConvnet-15	BCOP	43.70%	30.11%	19.85%	12.29%	-1.47%
	Cayley	45.05%	31.60%	20.32%	12.93%	-0.83%
	SOC (baseline)	47.72%	33.52%	21.89%	13.76%	(+0%)
	SOC + HH	**47.72%**	33.97%	22.45%	13.81%	+0.05%
	+ CR	47.61%	**34.54%**	**23.16%**	**15.09%**	**+1.33%**
LipConvnet-20	BCOP	39.77%	27.20%	17.44%	10.49%	-3.61%
	Cayley	39.68%	26.93%	17.06%	10.48%	-3.62%
	SOC (baseline)	46.86%	33.48%	22.14%	14.10%	(+0%)
	SOC + HH	47.71%	34.22%	22.93%	14.57%	+0.47%
	+ CR	**47.84%**	**34.77%**	**23.70%**	**15.84%**	**+1.74%**

Table 10: Results for provable robustness on the CIFAR-100 dataset using shallow networks. All of these results include Last Layer Normalization (LLN).

Architecture	Methods	Standard Accuracy	Provable Robust Acc. ($\rho =$)			Increase
			36/255	72/255	108/255	(108/255)
LipConvnet-25	BCOP	34.15%	21.57%	13.52%	7.97%	-5.89%
	Cayley	33.93%	21.93%	13.68%	8.19%	-5.67%
	SOC (baseline)	46.32%	32.87%	21.53%	13.86%	(+0%)
	SOC + HH	**47.70%**	34.00%	22.67%	14.57%	+0.71%
	+ CR	46.87%	**34.09%**	**23.41%**	**15.61%**	**+1.75%**
LipConvnet-30	BCOP	29.73%	18.69%	10.80%	6%	-7.52%
	Cayley	28.67%	18.05%	10.43%	6.09%	-7.43%
	SOC (baseline)	46.18%	32.82%	21.52%	13.52%	(+0%)
	SOC + HH	46.80%	33.72%	22.70%	14.31%	+0.79%
	+ CR	**46.92%**	**34.17%**	**23.21%**	**15.84%**	**+2.32%**
LipConvnet-35	BCOP	25.65%	14.88%	8.47%	4.30%	-8.95%
	Cayley	27.75%	16.37%	9.52%	5.40%	-7.85%
	SOC (baseline)	45.22%	32.10%	21.28%	13.25%	(+0%)
	SOC + HH	46.21%	32.80%	21.55%	14.13%	+0.88%
	+ CR	**46.88%**	**33.64%**	**23.34%**	**15.73%**	**+2.48%**
LipConvnet-40	BCOP	30.66%	18.68%	10.46%	5.92%	-6.07%
	Cayley	25.54%	14.91%	8.37%	4.40%	-7.59%
	SOC (baseline)	42.94%	29.71%	19.30%	11.99%	(+0%)
	SOC + HH	**45.84%**	**32.79%**	21.98%	14.07%	+2.08%
	+ CR	45.03%	32.57%	**22.37%**	**14.76%**	**+2.77%**

Table 11: Results for provable robustness on the CIFAR-100 dataset using deeper networks. All of these results include Last Layer Normalization (LLN).

Architecture	Methods	Standard Accuracy	Provable Robust Acc. ($\rho =$)			Increase
			36/255	72/255	108/255	(108/255)
LipConvnet-5	**SOC + HH$^{(2)}$**	46.61%	32.50%	21.34%	13.22%	+0.01%
	+ CR	**46.69%**	**33.22%**	**22.34%**	**14.30%**	**+1.09%**
LipConvnet-10	**SOC + HH$^{(2)}$**	47.47%	33.32%	21.84%	13.75%	-0.01%
	+ CR	**47.53%**	**34.52%**	**23.06%**	**15.07%**	**+1.31%**
LipConvnet-15	**SOC + HH$^{(2)}$**	47.19%	33.67%	22.36%	13.78%	-0.09%
	+ CR	**47.22%**	**34.04%**	**22.98%**	**15.28%**	**+1.41%**
LipConvnet-20	**SOC + HH$^{(2)}$**	**47.86%**	33.93%	22.44%	14.41%	+0.31%
	+ CR	47.54%	**34.32%**	**23.53%**	**15.54%**	**+1.44%**
LipConvnet-25	**SOC + HH$^{(2)}$**	**47.86%**	33.97%	22.78%	14.59%	+0.73%
	+ CR	47.50%	**34.38%**	**23.92%**	**15.92%**	**+2.06%**
LipConvnet-30	**SOC + HH$^{(2)}$**	46.23%	32.64%	21.95%	14.00%	+0.48%
	+ CR	**46.36%**	**33.20%**	**22.70%**	**14.85%**	**+1.33%**
LipConvnet-35	**SOC + HH$^{(2)}$**	**46.06%**	32.35%	21.33%	13.65%	+0.40%
	+ CR	45.78%	**33.24%**	**22.39%**	**14.78%**	**+1.53%**
LipConvnet-40	**SOC + HH$^{(2)}$**	43.81%	30.59%	20.08%	12.56%	+0.57%
	+ CR	**45.61%**	**32.50%**	**22.36%**	**14.84%**	**+2.85%**

Table 12: Results for provable robustness on CIFAR-100 using HH activation of Order 2 (σ_{Θ}). Increase (108/255) is calculated with respect to SOC baseline (from Tables 10, 11). All of these results include Last Layer Normalization (LLN).

Architecture	Methods	Standard Accuracy	Provable Robust Acc. ($\rho =$)			Increase
			(36/255)	(72/255)	(108/255)	(Standard)
LipConvnet-5	SOC (no LLN)	42.71%	27.86%	17.45%	9.99%	(+0%)
	SOC + LLN	**45.86%**	**31.93%**	**21.17%**	**13.21%**	**+3.15%**
LipConvnet-10	SOC (no LLN)	43.72%	29.39%	18.56%	11.16%	(+0%)
	SOC + LLN	**46.88%**	**33.32%**	**22.08%**	**13.87%**	**+3.16%**
LipConvnet-15	SOC (no LLN)	42.92%	28.81%	17.93%	10.73%	(+0%)
	SOC + LLN	**47.72%**	**33.52%**	**21.89%**	**13.76%**	**+4.80%**
LipConvnet-20	SOC (no LLN)	43.06%	29.34%	18.66%	11.20%	(+0%)
	SOC + LLN	**46.86%**	**33.48%**	**22.14%**	**14.10%**	**+3.80%**
LipConvnet-25	SOC (no LLN)	43.37%	28.59%	18.18%	10.85%	(+0%)
	SOC + LLN	**46.32%**	**32.87%**	**21.53%**	**13.86%**	**+2.95%**
LipConvnet-30	SOC (no LLN)	42.87%	28.74%	18.47%	11.21%	(+0%)
	SOC + LLN	**46.18%**	**32.82%**	**21.52%**	**13.52%**	**+3.31%**
LipConvnet-35	SOC (no LLN)	42.42%	28.34%	18.10%	10.96%	(+0%)
	SOC + LLN	**45.22%**	**32.10%**	**21.28%**	**13.25%**	**+2.80%**
LipConvnet-40	SOC (no LLN)	41.84%	28.00%	17.40%	10.28%	(+0%)
	SOC + LLN	**42.94%**	**29.71%**	**19.30%**	**11.99%**	**+1.10%**

Table 13: Results for provable robustness on the CIFAR-100 dataset with and without LLN